Within-host dynamics of mycoplasma infections: Conjunctivitis in wild passerine birds

Paul J. Hurtado *

Center for Applied Mathematics, 657 Frank H.T. Rhodes Hall, Cornell University, Ithaca, NY 14853, USA

ARTICLE INFO

ABSTRACT

The host–pathogen interaction drives infectious disease dynamics at the individual, population and community levels. Here I present and analyze a model of the vertebrate immune response to mycoplasma infections, and use it to identify which pathogen and host immune characteristics drive patterns of *Mycoplasma gallisepticum* (MG) infections in the house finch (*Carpodacus mexicanus*) and other passerine birds. I also address which host and pathogen characteristics most affect host infectiousness and survival. These results imply that much of the observed variation in the house finch likely arises from variation among birds in the effectiveness of their non-specific immune response to MG, and that the host and pathogen characteristics most likely to influence host infectiousness and survival are the intrinsic pathogen growth rate, the strength and efficiency of the non-specific immune response and characteristics affecting the effectiveness of the specific response. These findings suggest that molecular-level study of how MG and other mycoplasmas interact with a host's non-specific and inflammatory responses should reveal much about the relationships between host infectiousness, pathogen load, and disease symptoms in these systems.

1. Introduction

The host–pathogen interaction is at the core of every infectious disease system, and provides an important foundation from which to study infectious disease at the individual, population and ecosystem levels. Central to this interaction is the interplay between the pathogen and the host's immune defenses, which can largely determine (1) both short and long term consequences of infection for the host and (2) host infectiousness and pathogen transmission. The immune–pathogen interaction also mediates how various external factors act to shape the progression and consequences of an infectious disease.

The motivation for this paper is a bacterial disease caused by the pathogen *Mycoplasma gallisepticum* (MG), which has been the focus of many studies since its appearance in wild passerine birds in eastern North America around 1993 (Luttrell et al., 1996; Fischer et al., 1997; Dhondt et al., 1998; Hartup et al., 1998; Luttrell et al., 1998; Hochachka and Dhondt, 2000; Hartup et al., 2001a, 2001b; Altizer et al., 2004a, 2004b; Faustino et al., 2004; Hosseini et al., 2004; Kollias et al., 2004; Dhondt et al., 2005; Farmer et al., 2005; Hawley et al., 2005, 2005a; Hotchkiss, 2005; Lindstrom, 2005;

Sydenstricker et al., 2005; Altizer et al., 2006; Cherry et al, 2006; Dhondt et al., 2006; Hawley et al., 2006; Hochachka and Dhondt, 2006; Ley et al., 2006; Sydenstricker et al., 2006; Cooper et al., 2007; Dhondt et al., 2007a; Dhondt, 2007b; Hawley, 2007; Dhondt, 2008; Grodio, 2008; Hurtado, 2008; Hawley, 2010; Grodio et al., 2011). Originally known as a respiratory pathogen of domestic poultry, MG has been well studied prior to its jump to passerine hosts in the early 1990s. Its primary host is the house finch (*Carpodacus mexicanus*), a widespread species introduced into eastern North America from southern California in the early 1940s (Elliott and Aribib, 1953; Aldrich and Weske, 1978). MG can also infect the American goldfinch (*Carduelis tristis*) and other Carduline finches, and has been detected in various other bird species (Fischer et al., 1997; Mikaelian et al., 2001; Hartup et al., 2001a, DeCoste et al., pers. comm.). Disease symptoms include severe inflammation of the conjunctiva (the mucosal surface of the eye), lethargy, and in some cases death (Luttrell et al., 1998; Dhondt et al., 2005).

There are multiple reasons to study *M. gallisepticum* in wild birds. First, this disease shares many of the hallmarks of mycoplasmal infections in other organisms including some model organisms (rodents), other wildlife (e.g., some ungulates), domestic poultry, pigs and humans (Brown et al., 2005; Marco et al., 2009; Baseman and Tully, 1997; Hu, 2009; Messick, 2004). Second, this wildlife disease is relatively easy to study *in situ* since disease symptoms can be visually observed in wild birds and also since these organisms can be studied in captivity. Third,

* Present address: Mathematical Biosciences Institute, The Ohio State University, Jennings Hall, 3rd Floor, 1735 Neil Avenue, Columbus, OH 43210, USA. Tel.: +1 614 292 6159.
E-mail address: ph62@cornell.edu

this system provides an opportunity to study host–pathogen coevolution during the emergence of a novel infectious disease. Following its appearance during the early 1990s MG led to significant declines in the eastern population of the house finch and today continues to spread into western North America. The genomes of some MG strains have been sequenced and the functional genomics of MG and other mycoplasmas are fairly well understood (Papazisi et al., 2003; Blanchard and Browning, 2005). Furthermore, recent evidence shows that strains of MG circulating among house finches differ in virulence, which has changed over time.

Fig. 1 illustrates the range of disease progression among house finches using data from experimentally infected captive birds (Grodio, 2008; Grodio et al., 2011; Hawley, 2010). The typical course of infection in the house finch ranges from a very mild acute illness to a more persistent disease with prolonged severe inflammation. Symptomatic infections begin with a brief asymptomatic period followed by mild to severe inflammation of the mucosal tissues surrounding the eye and inside the eyelids (the conjunctiva). This diseased state may clear within a week or two, however in some individuals it can persist for months or may be so severe as to result in death (Sydenstricker et al., 2006; Kollias et al., 2004; Roberts et al., 2001). These persistent infections are typically symptomatic, although the existence of chronic asymptomatic infections has been put forth as one possible mechanism for interannual persistence of MG in wild house finch populations. Observations thus far suggest that the resolution of symptoms typically (though not exclusively) follows a reduction in pathogen load by the host's immune response.

The goal of this paper is to develop and analyze a dynamic model of the vertebrate immune response to a localized mycoplasma infection and use it to answer the following questions about *M. gallisepticum* in wild passerine birds. First, empirical study of this system has shown significant variation in the progression of *M. gallisepticum* infections within and between host species. Such variation is common in wildlife disease systems with multiple host species. To what extent can this variation be explained by a relatively simple model of the pathogen and host immune interaction? What aspects of this variation may result from factors not included this model? Second, preliminary data suggest that there has been some evolutionary change in virulence (i.e., the severity of host symptoms) among circulating strains of *M. gallisepticum* (Hawley et al., pers. comm.). Virulence evolution in this system is likely shaped by pathogen load, which drives host infectiousness (pathogen fitness), and by host disease symptoms, which drive host mortality risk and thus survival (host fitness). Which pathogen and host immune characteristics most affect host infectiousness and host mortality risk? Can likely targets for empirically detecting virulence-driven selection in the host or pathogen be identified using this model?

Mycoplasma infections are typically quite persistent and induce severe inflammation by eliciting a frustrated and ineffective host immune response. To quote Simecka (2005), "it is likely that almost every component of the host immune system is involved in the response to mycoplasma disease." In particular, both specific and non-specific immune responses are involved in controlling infections, and mycoplasmas may manipulate the host
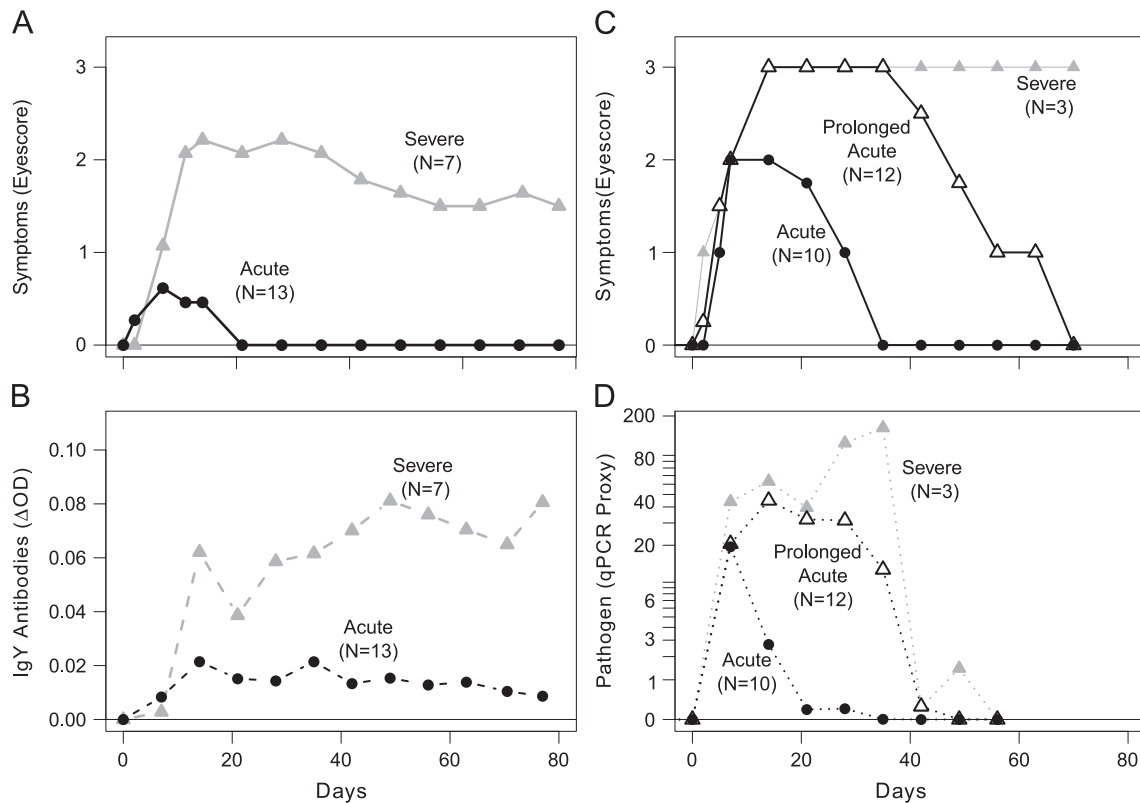

Fig. 1. *Mycoplasma gallisepticum* infections in the house finch (*Carpodacus mexicanus*) range from very mild to very severe. Panels on the left show symptoms (A) and antibody levels (B) for 20 individuals from the common garden experiment described in Hawley (2010) and Grodio et al. (2011). The means for groups are shown: the seven most severe infections from that experiment (*N* =40) and 13 that resolved symptoms of infection from the group (*N* =20) infected with a 2006 isolate of *M. gallisepticum*. Panels on the right show average symptoms (C) and approximate pathogen load (D) from a second experiment (Grodio, 2008; Grodio et al., 2011). Here the median values for three qualitatively similar groups are shown: mild acute infections, prolonged acute infections, and severe infections characterized by persistent, severe symptoms over the duration of the experiment. "Eye Score" is a standard measure of the severity of conjunctivitis (Kollias et al., 2004; Sydenstricker et al., 2006) and IgY is the avian equivalent of mammalian IgG.

immune response by interfering with regulatory pathways (Citti et al., 2005). Modeling the immune response to mycoplasmas poses a considerable challenge because so many aspects of the immune system contribute to controlling mycoplasma infections, and because some aspects of the pathogen–immune interaction are not well understood. The coarse grained modeling approach used here attempts to reduce that complexity by making functional categorizations of the various immune components and their main effects. The key benefit of this approach is that it yields a relatively simple, mathematically tractable model which captures the main biological processes that shape these immune–pathogen dynamics.

The remainder of the paper is organized as follows. Section 2 summarizes the key aspects of the host immune response to mycoplasmas, and a brief history of mycoplasmal conjunctivitis in wild birds. Section 3 introduces a mathematical model of the host immune response to a localized *M. gallisepticum* infection as well as the suite of further simplified models which are analyzed in the Results of Section 4. After describing the dynamics of these models, the remainder of Section 4 addresses how parameter value changes affect different measures of pathogen and host fitness. Section 5 concludes with a summary and discussion of the main results and their implications.

2. Biological background

It is known from observations of captive and wild individuals infected with *M. gallisepticum* that considerable variation in disease progression exists between and within host species, and between different pathogen strains (Dhondt, 2007b, 2008; Hawley, 2010). Many factors likely contribute to this variation by affecting the immune–pathogen interaction. These include pathogen strain, host genetics, nutrition, ambient temperature, time of year, host social status, and the route of initial infection—e.g., orally vs. directly into the conjunctiva (Dhondt, 2007b; Hawley, 2007, 2010; Altizer et al., 2006; Hawley et al., 2005a, Dhondt et al., pers. comm.).

2.1. Mycoplasmas and the host immune response

Mycoplasmas belong to the class of bacteria known as the Mollicutes (Edward and Kanarek, 1960; Edward and Freundt, 1967; Brown et al., 2007). Mollicutes are among the smallest known bacteria (as small as 0.3μm), tend to be highly host species specific, have no cell wall, and unlike many other bacteria cannot produce lipopolysaccharide (LPS), a cell wall component that elicits a strong immune response in vertebrates. As a group, mycoplasmas interact closely with host mucosal membranes and infections tend to be both persistent and accompanied by severe inflammation.

Based on what is known about the vertebrate immune response to mycoplasmas (Blanchard and Browning, 2005), the typical *M. gallisepticum* (MG) infection in house finches likely proceeds as follows. Once a small population of MG cells is introduced into the conjunctiva, individual cells must survive the first line of host immune defenses (e.g., resting macrophages, antimicrobial peptides, etc.) and attach to the surface of the epithelial cells lining the mucosal membrane (Luttrell et al., 1996). It is assumed that, in the absence of an immune response, the MG population would grow exponentially until reaching a maximum density determined by resource limitation and other physical constraints. During colonization of the host, close interaction with the host epithelial cells activates the non-specific immune components (e.g., macrophages) and induces the host's inflammatory response. The number and activity level of

phagocytic cells at the infection site increases, however these may be ineffective at killing MG without the presence of specific antibodies (Hickman-Davis et al., 1997; Simecka, 2005, pp. 485–493). This ineffective non-specific immune response slows, but does not stop, the growing pathogen population. Antigen-presenting cells associated with the non-specific immune response then activate specific immune components by transporting MG antigens into the lymphatic system. There they initiate B- and T-cell selection and maturation which later results in the production of MG-specific antibodies that allow phagocytic cells like macrophages to more effectively neutralize MG. This results in clearance of the infection unless MG evades the immune response (e.g., via surface antigen turnover, Citti et al., 2005) or the response is otherwise ineffective. As is commonly the case with mycoplasma infections, pathogen persistence is associated with sustained inflammation from the host's frustrated and ineffective immune response. In house finches, this includes visible signs of conjunctival inflammation accompanied by epithelial and lymphoid hyperplasia (Luttrell et al., 1996; Dhondt et al., 2005).

3. Model

3.1. Model equations

Based on the biological details in Section 2 and simplifying assumptions described in this Section, one can derive the innate (non-specific) immune response model described in Reynolds et al. (2006), which is extended here to include the adaptive (specific) immune response to mycoplasmas as described in Simecka (2005). The state variables represent the combined activity of various immune system components involved in the response to mycoplasma infections, grouped into functional categories as illustrated in Fig. 2. Scaled to reduce the number of parameters, the state variables are the pathogen density p, active non-specific (innate) immune components n, and progenitor cells y_0 that mature into active specific immune components y (e.g., maturing and antibody producing B-cells, respectively). The model equations are

$$\frac{dp}{dt} = k_{pg}p(1-p) - \frac{k_m p}{\mu_p + p} - K(y)np \qquad (3.1a)$$

$$\frac{dn}{dt} = \frac{n + k_p p}{x_n + n + k_p p} - \mu_n n \qquad (3.1b)$$

$$\frac{dy_0}{dt} = \frac{(np)^\alpha}{x_y^\alpha + (np)^\alpha} - \mu_{y0} y_0 \qquad (3.1c)$$

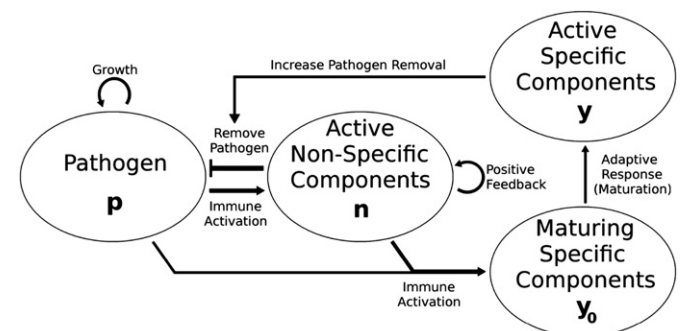$$\frac{dy}{dt} = \mu_{y0} y_0 - \mu_y y \qquad (3.1d)$$

Fig. 2. Model variables and main interactions included in the immune response Model (3.1).

where $K(y)$ is an increasing function of y with $K(0) > 0$. The unscaled model equations and their relationship to the model by Reynolds et al. (2006) are given in Appendix A.

The pathogen population is assumed to follow Eq. (3.1a), which assumes exponential growth at low pathogen density and an upper limit to pathogen density in the absence of an effective immune response. This is modeled as logistic growth with intrinsic growth rate k_{pg} in the absence of a host immune response (pathogen units have been scaled to maximum density $p = 1$ as detailed in Appendix A). The second term in Eq. (3.1a) models the ability of local (unactivated) immune defenses to neutralize an initially small population of invading pathogen as detailed in Reynolds et al. (2006).

The activated non-specific immune components n (see Eqs. (3.1a) and (3.1b)) include phagocytic and antigen-presenting cells like macrophages as well as other cells like heterophils (avian neutrophils). Activation of innate immune components results from both the presence of pathogens and some positive feedback, with deactivation occurring at rate μ_n. Together, they are assumed to activate the specific immune response (see Eq. (3.1c)) and to neutralize pathogens at per-capita rate $K(y)$. This removal rate is increased by the actions of the specific immune response, e.g., by the binding of antibodies to MG.

To incorporate the specific immune response, variables representing the maturing (y_0) and active (y) specific immune components are modeled with Eqs. (3.1c) and (3.1d). This assumes that the primary role of the specific immune response is to produce antibodies that enhance the efficiency of pathogen removal by innate immune components (e.g., phagocytic cells). The first term in Eq. (3.1c) models the activation of the specific immune components y_0 by antigen-presenting cells during an active infection. Activation is modeled using a saturating response to the level of pathogen p and innate immune activity n. Once activated, maturation occurs at rate μ_{y0} to produce specific immune components which then decay at rate μ_y. Mathematically, the maturation process simply introduces a delay in the production of active specific immune components (e.g., antibodies).

Though not included in Eqs. (3.1), the symptoms of disease appear to largely result from the host immune response, yet it is unknown whether these symptoms harm or benefit the pathogen, nor whether they help or hinder the immune response. For this work, it is assumed that the immune–pathogen dynamics are largely unaffected by disease symptoms, and that those symptoms are generated by a combination of both pathogen and immune activity as detailed in Section 4.4.

3.2. Simplified models and important subsystems

In formulating Model (3.1) the complexity of the vertebrate immune system is simplified by adopting a "top down" perspective that highlights how the immune system functions during mycoplasma infections. Many biological questions about the immune response to mycoplasmas can therefore be framed as mathematical questions about the dynamics of Eqs. (3.1), but despite this model's relative simplicity it only permits limited mathematical analysis.

In order to describe the dynamics of Model (3.1) beyond those limited analytical results, the dynamics of a suite of simpler models, which either approximate Eqs. (3.1) or are key subsystems of that model, are also presented. Computational results are also provided to illustrate the immune–pathogen dynamics of Model (3.1) for particular parameter regimes (see Table 1 in the next section).

The simplified models considered in this section primarily arise from the fact that different immune processes occur across a wide range of time scales (see Segel and Perelson, 1991 and Appendix B). It is therefore assumed that the non-specific immune activity (n) rapidly responds to changes in pathogen density (p), which itself changes quickly relative to the slower dynamics of the specific immune response (y).

The dynamics of these simplified models are presented in the next section as follows. The section begins by describing the pathogen dynamics in the absence of the host immune response. Then the dynamics of the innate response are described by considering the p–n subsystem in the absence of a changing specific immune response, i.e., $K(y) = K_{ny}$ is treated as a constant (see Fig. 2). This approximates the fast time scale dynamics of Model (3.1). Using standard separation of time scales techniques, the slow time scale dynamics can be approximated by using a simplified model which combines the p–n dynamics into a single

Table 1
Variables and parameter values of the scaled model given by Eq. (3.1). These values are based on the unscaled model parameters in Appendix A, Table A1. Time units are hours unless otherwise stated.

	Value	Description
Variable		
p	0–1	Rescaled pathogen density
n	$0-1/\mu_n$	Rescaled active innate components
y_0	$0-1/\mu_{y0}$	Rescaled maturing specific immune components
y	$0-1/\mu_y$	Rescaled active specific immune components
t	.	Rescaled damage from the immune response
Parameter		
k_{pg}	0.1	Pathogen growth rate
k_m	1.5×10^{-8}	Maximum removal by local innate components
μ_p	1×10^{-8}	Half-saturation constant for local innate components
K_{min}	> 0	$K(0)$; Baseline active innate pathogen removal rate
K_{max}	$> K_{min}$	Maximum removal rate, specific components present
θ	6	Determines steepness of $K(y)$ at $y = x_{ny}$
x	200	Half-saturation value for activation of specific response
x_y	8.29×10^{-6}	Half-saturation constant for pathogen removal rate $K(y)$
k_p	2.5×10^9	Pathogen activation of the innate response
x_n	199	Half-saturation value for activation of innate response
μ_n	0.05	Rate of active innate component loss
α	6	Determines response steepness at half-saturation value x_y
μ_{y0}	0.0037	Maturation rate of specific immune components
μ_y	0.0016	Rate of specific immune component loss

equation governing the pathogen dynamics and a second equation governing the dynamics of the specific immune response (this simplified, slow time scale model is accordingly referred to as the p–y model).

3.3. Model parameterization

Parameter values for Model (3.1) are shown in Table A1, and are determined by the scaling equations and unscaled model parameter values are given in Appendix A. These values are used to motivate certain simplifying assumptions, and to illustrate dynamics. Each parameter represents a particular biological quantity and values for those quantities have been chosen based on empirically derived quantities, where possible. The remaining parameter values were chosen to yield model dynamics similar to experimentally observed infection dynamics (Dhondt et al., 2005; Dhondt, 2008; Kollias et al., 2004; Sydenstricker et al., 2005, 2006). Because relatively few details are known about the avian immune system, many parameter values were based on those in Reynolds et al. (2006).

4. Results

4.1. Establishing the infection

The very early stages of infection are largely free from control by the host's immune response, and follow the single equation

$$\frac{dp}{dt} = k_{pg}p(1-p) - \frac{k_m p}{\mu_p + p} \tag{4.1}$$

Once a naive host is inoculated (density $p(0) \ll 1$), the pathogen population must overcome the host's baseline immune defenses in order to persist and proliferate. This first line of defense is modeled by the second term in Eq. (4.1) and affects the host–pathogen dynamics in two ways: First, it may cause a strong Allee effect for the pathogen population where initial densities below a critical size p_{crit} decline toward zero instead of increasing and establishing an infection. Second, it reduces the maximum attainable pathogen density ($p_{max} \leq 1$) by decreasing an important threshold quantity, the *effective intrinsic growth rate* of the pathogen (see Appendix C),

$$r_0 \equiv k_{pg} - k_m/\mu_p \tag{4.2}$$

The relationship between the strength of these baseline immune defenses (i.e., the magnitude of k_m) and the two phenomena just mentioned are illustrated in Fig. 3 and can be described as follows.

In the absence of these defenses (i.e., if $k_m = 0$), the pathogen population follows simple logistic growth toward $p_{max} = 1$ (here $r_0 \equiv k_{pg}$ is positive). Increasing the strength of the baseline immune defenses $k_m > 0$, the attracting pathogen density p_{max} decreases toward $p = 1 - \mu_p$ while a third equilibrium value $p_{crit} < 0$ increases toward 0 and r_0 decreases toward 0. Further increasing k_m results in r_0, p_{max} and p_{crit} simultaneously passing through 0, $1 - \mu_p$ and 0, respectively (see Fig. 3B). This leaves the threshold value p_{crit} positive, with both the maximum pathogen density p_{max} and the state of health ($p = 0$) locally attracting. A necessary condition here and in Model (3.1) for having bistability with the origin is that $r_0 < 0$. Increasing k_m even further causes p_{crit} and p_{max} to move toward one another (see Fig. 3B,C) until they meet and vanish, leaving the host completely immune to infection. See Appendix C for additional details.

The inclusion of these baseline immune defenses (i.e., assuming $k_m > 0$) can lead to interesting dynamics under Model (3.1), but they also obscure how other immune components help
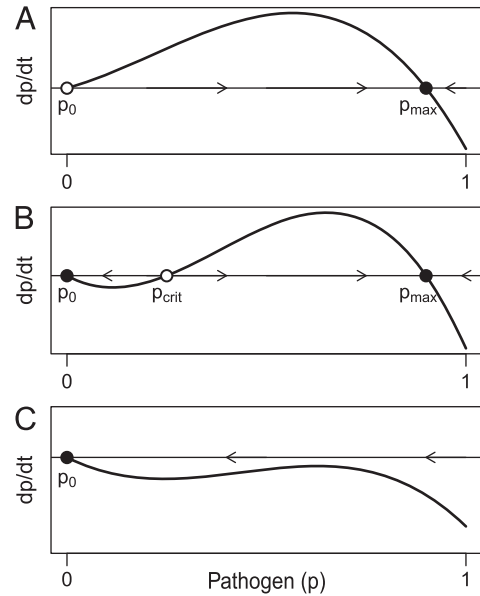

Fig. 3. Pathogen dynamics in the absence of an active immune response (i.e., following Eq. (4.1)). Three possibilities exist, and depend on the relative strength of the host's baseline immune defenses k_m which here increases from low (panel A) to very high (C). In panel A, $k_m \approx 0$ so the effective intrinsic growth rate r_0 is positive and the dynamics are similar to logistic growth. Panel B shows the result of increasing k_m until r_0 becomes negative. This results in a strong Allee effect (and bistability) where initial pathogen densities must be higher than p_{crit} (an unstable equilibrium) to increase toward the steady state density p_{max}. In panel C, further increases in k_m result in the loss of the persistence steady state p_{max}, leaving the host completely immune to infection. The transitions between these different states occur via a transcritical bifurcation (A to B) and a saddle-node bifurcation (B to C), as detailed in Appendix C.

determine different infection outcomes. To clarify the role of other immune components, results presented in Sections 4.2 and 4.3 first assume negligible baseline immune defenses ($k_m = 0$), and then describe how those dynamics change by including such defenses ($k_m > 0$).

4.2. Early pathogen control: non-specific immunity

The non-specific immune components (n) play two important roles during a newly established infection: they directly eliminate pathogen and help activate the specific immune response. During a mycoplasma infection, a susceptible host's non-specific immune response is often ineffective and requires the specific immune response to clear the infection (Simecka, 2005). Accordingly, the non-specific immune response is important in shaping the timing, severity and persistence of infections across different hosts and host species.

To describe how the non-specific immune response shapes infection dynamics, the fast time scale dynamics of Model (3.1) can be approximated by holding the specific immune response (y) constant. In the full Model (3.1), y and $K(y)$ both change relatively slowly during an active infection. Defining the constant $K_{ny} = K(y)$, Model (3.1) becomes

$$\frac{dp}{dt} = k_{pg}p(1-p) - \frac{k_m p}{\mu_p + p} - K_{ny}np \tag{4.3a}$$

$$\frac{dn}{dt} = \frac{n + k_p p}{x_n + n + k_p p} - \mu_n n \tag{4.3b}$$

If baseline immune defenses are negligible (i.e., if $k_m = 0$), then there is no Allee effect. An infection in this case will always approach either a positive steady-state pathogen density $p_* > 0$ and level of immune activity $n_* > 0$, or the infection will be

cleared by a self-sustaining inflammatory response with steady state $n_n > 0$ (see Appendix C and Reynolds et al., 2006 for details). Since self-sustained inflammatory responses are currently unknown in the motivating biological system, the focus now turns to the persistence steady state (p_*, n_*) to determine under what conditions p_* is significantly greater than 0.

Figs. 4A and B (where $k_m = 0$) show how slowly increasing the net effectiveness of the immune response (K_{ny}) reduces the attracting pathogen level p_* in a nearly linear fashion until p_* is very near 0 (see arrow, Fig. 4B). Interestingly, any further increases in K_{ny} allow the pathogen to persist at very low levels relative to the maximum possible densities. This persistence results from the absence of an Allee effect when $k_m = 0$ and from the very low saturation threshold ($x_n/k_p \approx 0$) for the activation of the non-specific response according to Eq. (4.3b) and Table 1. If activation of the non-specific response saturates at higher pathogen densities, then this transition is far less abrupt (compare Figure panel 4A with C-F).

If baseline immune defenses are sufficiently strong ($k_m > 0$), these dynamics change as expected from Section 4.1. Baseline immune defenses can induce an Allee effect that hinders or prevents the establishment of infection and allows complete pathogen clearance by the immune response. Increasing K_{ny}, the dynamic changes may be similar to the $k_m = 0$ case, however if baseline immune defenses are very strong such increases can yield a more abrupt clearance of the pathogen via a saddle-node bifurcation as shown in Fig. 4E. These baseline immune defenses also reduce the attracting pathogen density p_*, although this reduction is very small for biologically relevant parameter values. For more details regarding the Model (4.3) dynamics see Appendix C.

4.2.1. Simplifying the p-n subsystem

In addition to the biological motivations for discussing the dynamics of the p–n subsystem (4.3), the results in Section 4.2 help simplify Model (3.1) to clarify how the specific immune response (y) shapes infection outcomes. To further simplify Models (3.1) and (4.3) two additional assumptions are made. First, since self-sustained inflammatory responses are unknown in this system, assume a negligible amount of positive feedback in the activation of the non-specific immune response, so

$$\frac{dn}{dt} = \frac{k_p p}{x_n + k_p p} - \mu_n n \qquad (4.4)$$

This rules out the potential for a self-sustaining inflammatory response (see Appendix C.3).

Second, the non-specific immune response (n) responds rapidly to changes in other model variables for parameter values like those in Table 1. This fast non-specific response together with
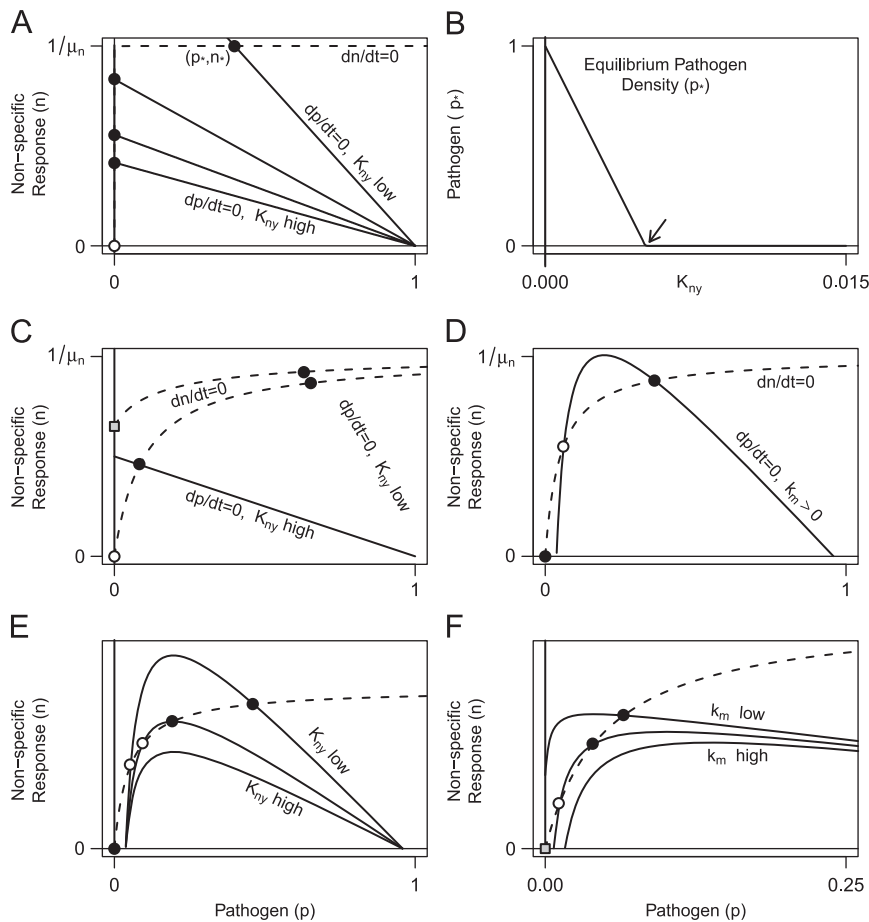

Fig. 4. Example n- and p-nullclines (solid and dashed curve, respectively) illustrating the dynamics of the p–n subsystem (4.3). Equilibria (filled=stable, empty=unstable) occur where the nullclines intersect. Panel A shows the possible dynamics assuming values similar to those in Table 1 with $k_m = 0$ (no bistability). Panel C shows the nullclines and equilibria more clearly using different values. If the self-sustaining inflammatory response value $n_n \equiv 1/\mu_n - x_n$ is positive (shaded square in C), then either that state or the unique persistence equilibrium (p_*) is attracting depending on whether or not $p_* > 0$. If $n_n < 0$, then the only equilibria are the (unstable) origin and the (stable) persistence equilibrium p_* (see text and Appendix C for stability conditions). Panel B shows how p_* changes with increasing immune efficiency K_{ny} assuming $k_m = 0$ and $n_n < 0$, using a broader range of K_{ny} values than shown in A. Panels D–F shows how assuming $k_m > 0$ introduces multiple interior equilibria ($p_*, n_* > 0$) and can lead to bistability. Panel E and F illustrate how the nullclines (and persistence equilibria) change with increasing efficiency of the specific immune response (increasing K_{ny}) and increasing strength of baseline immune defenses (increasing k_m), respectively.

Eq. (4.4) implies that n rapidly tracks changes in pathogen density p according to the quasi-steady state value

$$\mathbf{n}(p) = \frac{1}{\mu_n}\left(\frac{k_p p}{x_n + k_p p}\right) \tag{4.5}$$

obtained by assuming the right-hand side of Eq. (4.4) equals 0 (see Appendix B). Hence, the dynamics of this simplified p–n subsystem can be approximated by the single equation

$$\frac{dp}{dt} = k_{pg}p(1-p) - \frac{k_m p}{\mu_p + p} - K_{ny}\mathbf{n}(p)p \tag{4.6}$$

Since Eq. (4.6) is a one dimensional ODE, one can analyze its dynamics completely. As detailed in Appendices C.3 and C.4, it behaves just like the simplified p–n model (Eqs. (4.3a) and (4.4)) except there are no cycling dynamics. Any equilibrium pathogen value p_* of the simplified p–n model is necessarily an equilibrium of Eq. (4.6), thus there can be up to three equilibria in the unit interval, in addition to the origin (see Fig. C1, Appendix C.4). The stability of the origin depends on the sign of r_0, as expected, and no self-sustained inflammatory response is possible in the absence of pathogen (i.e., $\mathbf{n}(0) = 0$). Any equilibrium pathogen density p_* under Eq. (4.6) is locally stable if the slope of the simplified p–n model's n-nullcline is greater than that of the p-nullcline at p_*, and is unstable otherwise. The largest such equilibrium (always less than 1) is always stable when positive.

4.3. Pathogen persistence and the specific immune response

This section describes how the specific immune response shapes the outcome of infection when the non-specific response fails to clear the infection on its own. In doing so two questions are addressed: First, when does the steady state pathogen density p_* correspond to high or very low pathogen densities? Second,

how do different levels of specific and non-specific immune efficacy affect p_*?

Using Eq. (4.6), the role of the specific immune response (y) in Model (3.1) can be described by making the additional simplifying assumption that the delay in activating the specific immune response is negligible. Simulation results suggest that this affects the timing of the specific immune response, but has little effect on the asymptotic dynamics. These assumptions yield the simplified slow time scale model

$$\frac{dp}{dt} = \left(k_{pg}(1-p) - \frac{k_m}{\mu_p + p} - K(y)\mathbf{n}(p)\right)p \tag{4.7a}$$

$$\frac{dy}{dt} = \frac{(\mathbf{n}(p)p)^\alpha}{x_y^\alpha + (\mathbf{n}(p)p)^\alpha} - \mu_y y \tag{4.7b}$$

which has a single immune response variable y. Here the efficiency of pathogen removal $K(y)$ increases with increasing y, and the quasi-equilibrium value of the non-specific immune response $\mathbf{n}(p)$ is given by Eq. (4.5). As a working example, assume $K(y)$ is sigmoidal

$$K(y) = \left(K_{min} + \frac{(K_{max} - K_{min})y^\theta}{x^\theta + y^\theta}\right) \tag{4.8}$$

where the minimum value $K(0) = K_{min}$ corresponds to the pathogen removal rate of the non-specific immune system alone ($y = 0$), and K_{max} is the maximum pathogen removal rate.

The course of infection under Model (3.1) can be divided into two stages: an early acute phase largely determined by the p–n subsystem dynamics, followed by either clearance or persistence of the infection according to the dynamics of the p–y model (4.7). Whether or not an acute infection is cleared by the specific
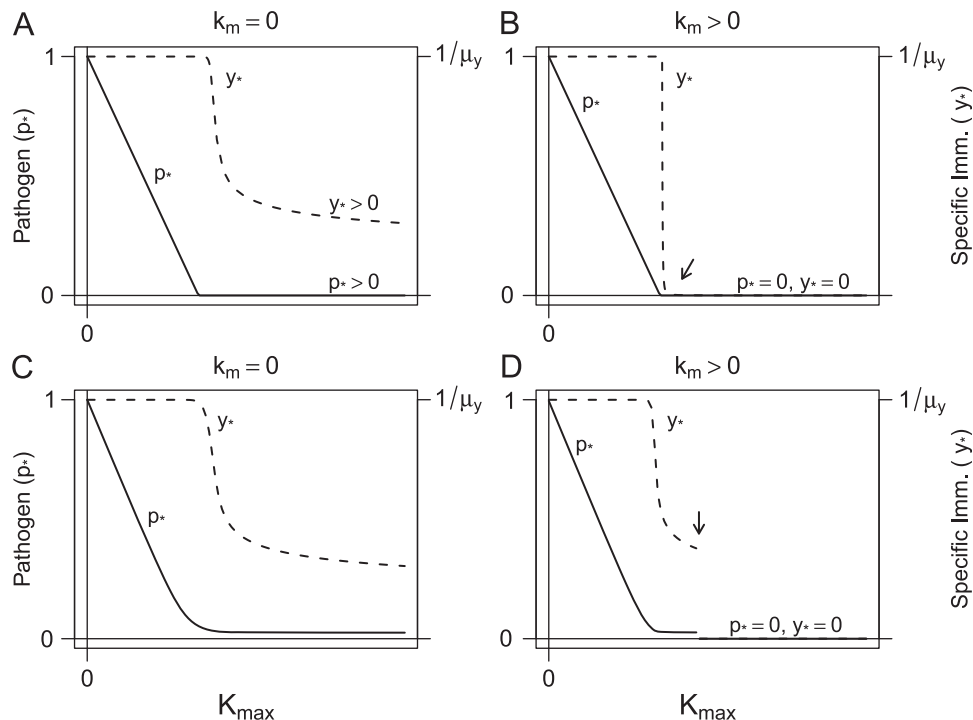

Fig. 5. Examples of how the specific immune response efficiency (K_{max}) and an Allee effect ($k_m > 0$) shape infection outcome under the p–y model (4.7). Steady state pathogen density p_* and specific immune activity y_* are shown for a range of K_{max} values ($K_{min} = 0$). Panel A, B show the dynamics without ($k_m = 0$) and with ($k_m > 0$) an Allee effect. Panels C, D show qualitatively equivalent dynamics to A, B. Increasing K_{max}, p_* decreases almost linearly until p_* yields diminishing rates of immune activation. With no Allee effect ($k_m \approx 0$), additional increases in K_{max} permit low-level pathogen persistence and a sustained immune response ($p_*, y_* > 0$). With an Allee effect ($k_m > 0$), clearance can occur. The transition between persistence and clearance can be sensitive to parameter changes and initial pathogen densities and involves a homoclinic bifurcation that abruptly expands the basin of attraction for the pathogen-free state near the transition (see Appendix D, Fig. D1 for details). Parameters: See Table 1. Panels B, D use $k_m = 1.5 \times 10^{-8}$ and $k_m = 4.8 \times 10^{-4}$, respectively. Panels C, D use $x_n = 0.01k_p$, $x_y = 4.15 \times 10^{-1}$. Initial conditions are $p(0) = 0.1$, $y(0) = 0$.

response depends largely on the efficiency of the specific response $K(y)$ and whether or not an Allee effect is present.

To describe the immune-pathogen dynamics under Model (4.7) first consider the case where baseline immune defenses are negligible ($k_m=0$, no Allee effect). In this case, there is always exactly one pathogen persistence steady state ($p_* > 0$, $y_* > 0$) that is always stable. More generally it can be shown that stability is guaranteed in this case whenever the activation rate of the specific immune response (first term in Eq. (4.7b)), the quasi-steady state of the non-specific immune response $\mathbf{n}(\cdot)$ and the efficiency of pathogen removal $K(\cdot)$ are all increasing functions at the equilibrium p_* (see Appendix D for details). As shown in Fig. 5A, this $p_* > 0$ may correspond to a high or very low pathogen density and requires a sustained immune response $y_* > 0$.

To highlight two transitions related to pathogen clearance and persistence, Fig. 5 shows how the steady state pathogen density p_* changes with increasing K_{max} in the presence or absence of an Allee effect. Increasing K_{max} from near K_{min} initially gives a near-linear decrease in pathogen density p_*. Eventually, p_* is small enough to decrease immune activation rates below their saturation thresholds. Beyond this transition, immune activity (y_*) decreases but pathogen density p_* changes little (see Fig. 5A,C).

The presence of an Allee effect ($k_m > 0$, Fig. 5B,D) introduces the potential for a second, more abrupt transition (see Fig. 5D) associated with a homoclinic bifurcation described in Appendix D.2. Similar to Fig. 4E, increasing K_{max} increases the Allee threshold and decreases p_*. Here, however, the basin of attraction for the pathogen-free state ($p = 0$, $y = 0$) can very suddenly grow to encompass nearly all biologically plausible initial conditions. Beyond this transition, the outcome of infection is complete clearance of the pathogen following the acute phase of infection.

Importantly, whether the outcome of infection is clearance or low-level persistence has major consequences for the host when disease symptoms are immune mediated, or when the immune response is otherwise costly (compare the two cases in Fig. 5). Under such circumstances, immune-mediated disease symptoms may increase host mortality risk or otherwise impact host fitness during persistent infections despite very low pathogen levels.

To more precisely describe how these dynamics depend on model parameters, consider the nullclines of Model (4.7)

$$g_p(p) = K^{-1}\left(\frac{k_{pg}(1-p) - \dfrac{k_m}{\mu_p + p}}{\mathbf{n}(p)}\right) \tag{4.9a}$$

$$g_y(p) = \frac{1}{\mu_y} \frac{(\mathbf{n}(p)p)^\alpha}{x_y^\alpha + (\mathbf{n}(p)p)^\alpha} \tag{4.9b}$$

where $K^{-1}(\cdot)$ is the inverse of $K(y)$.

For $k_m \geq 0$, the y-nullcline $g_y(p)$ is a monotone increasing function of p (approximately sigmoidal) with maximum value $1/\mu_y$. The shape of the p-nullcline $g_p(p)$ is more variable due to the bounded nonlinear function $K(y)$.

To see how different parameters shape the p-nullcline given by Eq. (4.9a), define

$$F(p) = \left(k_{pg}(1-p) - \frac{k_m}{\mu_p + p}\right)\Big/ \mathbf{n}(p) \tag{4.10}$$

so that the p-nullcline can be written as $g_p(p) = K^{-1}(F(p))$. Since $K(y)$ is a nonlinear (sigmoidal) function with the finite range [K_{min}, K_{max}), it follows that $K^{-1}(\cdot)$ is also nonlinear and that $g_p(p)$ is only defined for values of p where $F(p) \in [K_{min}, K_{max})$. Fig. 6 illustrates how this restricts the domain of $g_p(p)$ which for $K(\cdot)$ given by Eq. (4.8) results in a discontinuous p-nullcline defined on a domain of one to three disconnected intervals.
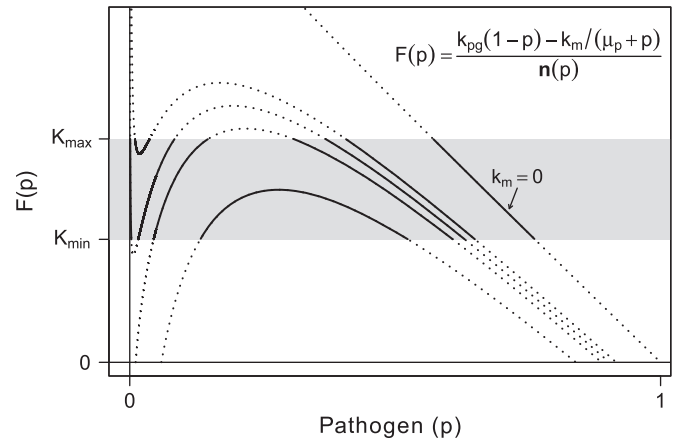

Fig. 6. The p-nullcline $g_p(p) \equiv K^{-1}(F(p))$ (4.9a) under the p–y model (4.7) is only defined for p values where $F(p)$ (4.10) falls within the range of $K(\cdot)$ (i.e., between K_{min} and K_{max}, shaded gray above). If baseline immune defenses are negligible ($k_m=0$, top curve), the domain of $g_p(p)$ is a single interval and the shape of $g_p(p)$ reflects the shape of $K(y)$ (cf. Fig. 7A). If $k_m > 0$, the domain of $g_p(p)$ may include two or more intervals (see the middle three curves). Over the lower interval(s) $g_p(p)$ is typically increasing (see Fig. 7D), or may have a local minimum between vertical asymptotes (see second highest curve here, and solid black curve in Fig. 7B). Where $g_p(p)$ is defined, it is increasing (or decreasing) wherever $F(p)$ is increasing (or decreasing, respectively), since $K^{-1}(\cdot)$ is strictly increasing on its domain [K_{min}, K_{max}].

Fig. 7 shows multiple instances of the p-nullcline (solid curves) for a range of K_{max} values. If baseline immune defenses are negligible ($k_m=0$), the p-nullcline (4.9a) is a decreasing function with domain (p_{lo}, p_{hi}). If $k_m=0$, then $F(p)$ is linear. Therefore, p_{lo} is determined by K_{max} (i.e., p_{lo} decreases as K_{max} is increased) and p_{hi} is determined by K_{min} (see the $k_m=0$ curve, Fig. 6) for any strictly increasing function $K(\cdot)$ with range (K_{min}, K_{max}]. As shown in Fig. 7A, the p-nullcline intercepts the p axis at p_{hi} and approaches ∞ on the lower end of this domain as p decreases toward p_{lo}.

If $k_m > 0$ (see the four lower curves in Fig. 6 and see Fig. 7B,D) the p-nullcline can be highly nonlinear which allows the p–y model to have multiple equilibria associated with low pathogen levels and instances of bi- and multi-stability including bistability between the persistence steady state and the origin (see Fig. 7). Some of these equilibria can undergo a Hopf bifurcation resulting in low-level pathogen-immune cycling, although simulations suggest cycling dynamics are rare or of small amplitude for biologically relevant parameter values. In dynamical systems terms, these new dynamics arise from transcritical bifurcations involving the origin, from saddle-node bifurcations in the interior of the positive quadrant, and from other bifurcations associated with a homoclinic bifurcation near a generalized Hopf bifurcation (see Appendix D).

These results suggest the following about the immune–pathogen dynamics under the simplified Models (4.7) and (3.1). First, pathogens with higher growth rates k_{pg} will have both higher steady state pathogen density p_* and result in more immune activity y_*. Second, low pathogen removal efficiency (e.g., reduced $K(y)$) yields both higher pathogen load and elevated immune activity. These results also highlight the synergistic nature of how the vertebrate immune system responds to infection, and the potential for nonintuitive dynamics to arise from even relatively simple models of that response.

4.4. Determinants of host infectiousness and mortality risk

We would like to know which pathogen and host characteristics most affect pathogen fitness (host infectiousness) and host fitness (host mortality risk). Here fitness is defined by two
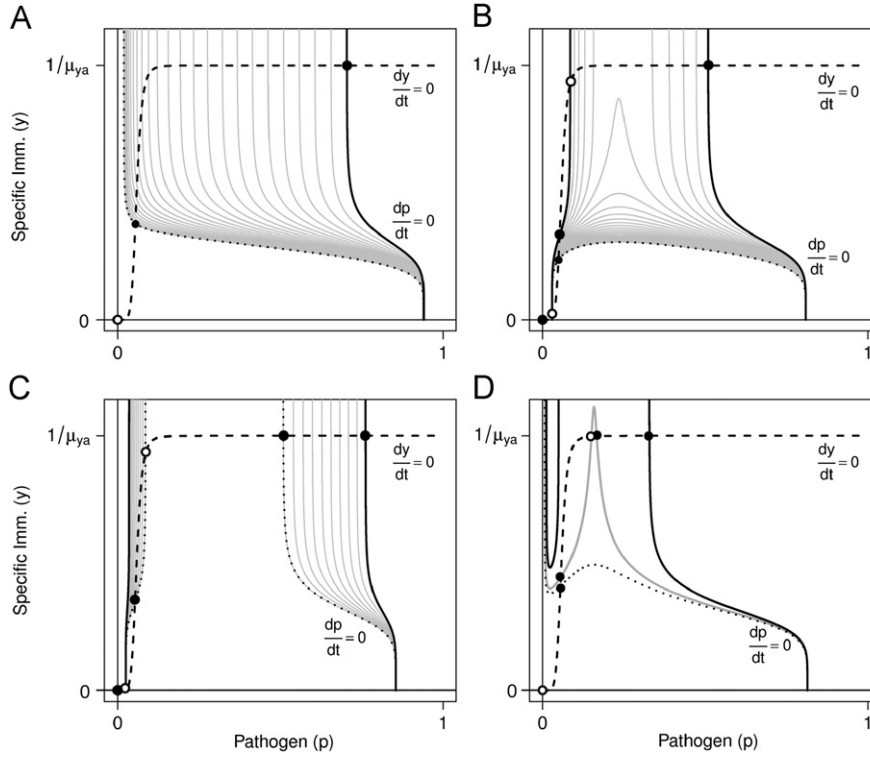
Fig. 7. Nullclines of the p–y model (4.7) illustrating the kinds of dynamics possible when $k_m=0$ (panel A) and when $k_m>0$ (panels B–D). Multiple instances of the p-nullcline (solid curves) are shown but only one instance of the y-nullcline (dashed curve). Gray curves indicate how the p-nullcline changes as K_{max} is increased with the solid black curve corresponding to the lowest value of K_{max} and the dotted curve the highest. Note vertical asymptotes at some boundaries of the p-nullcline's multi-interval domain (see Fig. 6).

important quantities. First, it is assumed that host infectiousness is given by total pathogen load (pathogen fitness) over the duration of the infection, given by

$$\pi(T) = \int_0^T p(t)\,dt \tag{4.11}$$

where time T is when the host dies or recovers (although see Lange and Ferguson, 2009; Holt and Barfield, 2006; Pepin et al., 2010 for other possible measures of pathogen fitness). Second, to quantify host survival, host death is modeled as a random process. In house finches, host mortality risk increases with disease symptoms that result from tissue damage and inflammation caused by the interaction between host immune components and pathogen (Faustino et al., 2004; Hochachka and Dhondt, 2000). Therefore the time an infected host dies is defined as the random variable T_{death}, given by

$$\mathbb{P}(T_{death} \leq T) = \exp\left(-\int_0^T \lambda(t)\,dt\right) \tag{4.12}$$

where the mortality rate $\lambda(t) \equiv cU(t)$ is assumed to be some function of the pathogen load p, non-specific response n and specific response y (thus $U(p,n,y)$ is a proxy for how disease symptoms affect survival) times a scaling constant c. The effect of disease on host fitness is quantified by the probability of surviving to day $T=40$, given by

$$\mathbb{P}_s \equiv 1 - \mathbb{P}(T_{death} \leq 40) \tag{4.13}$$

To identify which pathogen and host characteristics most strongly influence the two fitness quantities $\pi(T)$ and $\mathbb{P}_s$, a sensitivity analysis is used to determine how each changes with changing parameter values. Here the (relative) sensitivity of

quantity R to changes in parameter q is

$$S_q(R) = \frac{\partial R}{\partial q}\frac{1/R}{1/q} \tag{4.14}$$

Since the duration of infection T (time to host recovery or death) is highly variable, these parameter sensitivities for $\pi(T)$ are shown as curves over a range of T values, or *sensitivity profiles* with respect to T. In the case of $\mathbb{P}_s$, parameter c is largely unknown however it has no effect on the parameter ranks as determined by their respective relative sensitivies (as shown below in this section). These sensitivities are therefore computed for a convenient value of c then normalized to compare across different cases of $\lambda(t)$.

Fig. 8 shows pathogen fitness sensitivities for two instances of Model (3.1). The comparison between parameter sensitivities before and after control by the specific immune response ($T \approx 15$ in Fig. 8C) suggests that whether or not individual pathogen characteristics are likely to respond to selection depends on whether transmission typically occurs before or after the specific immune response. If the host dies or otherwise ceases to be infectious prior to the specific response, pathogen fitness is most sensitive to changes in the pathogen's intrinsic growth rate k_{pg}, the loss rate of non-specific immune components μ_n and the effectiveness of the non-specific immune response in removing pathogen K_{min}. Otherwise, if sufficiently many new infections arise from infectious hosts with active specific immune responses, selection may act on additional pathogen characteristics that affect the activation rate of the specific response or its effectiveness in removing pathogen.

To identify the host and pathogen characteristics that influence host survival, let us consider the relative sensitivity of host survival $\mathbb{P}_s$ (4.13) to changes in parameters over a range of virulence scalar values, c, and for multiple possible forms of
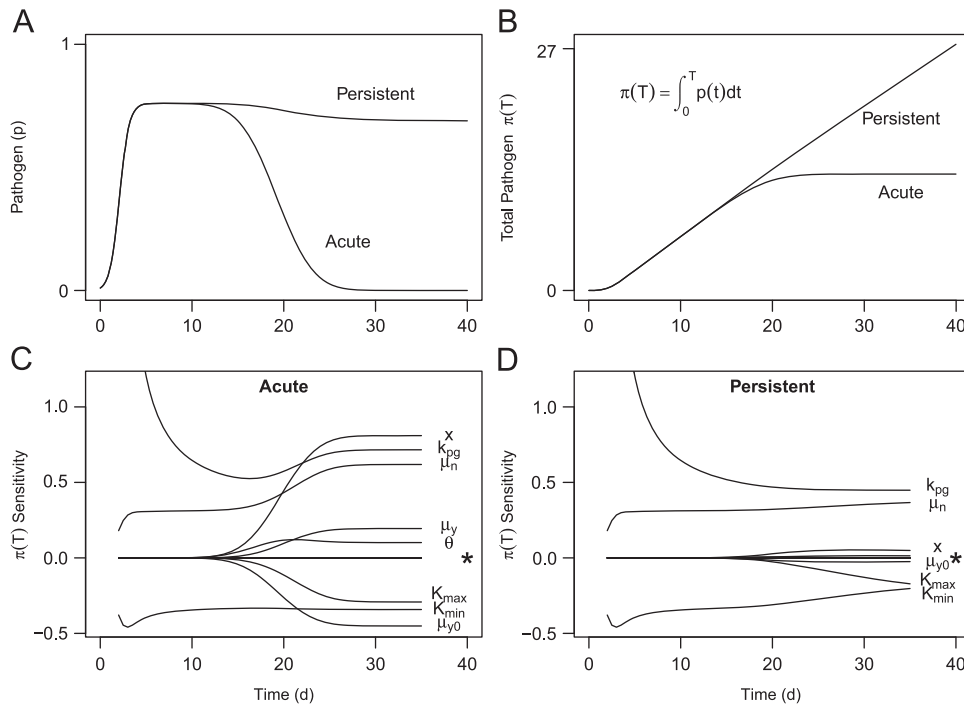
Fig. 8. Sensitivity profiles for Model (3.1) showing how pathogen fitness (total pathogen load $\pi(T)$ (4.11)) responds to small changes in the parameter values in Table 1 with $K_{min} = 0.0012$. Sensitivities are shown for a range of times T, as total pathogen load depends on the duration of infection which may be shortened by host death. Panel A shows pathogen dynamics for an acute infection ($K_{max} = 0.0075$) and a persistent infection ($K_{max} = 0.00156$). Panel B shows the total pathogen load for each case. The curves in C, D are relative sensitivities for each parameter, computed over a range of T values (see text). Here ∗ indicates parameters with sensitivities near 0. The primary determinants of infectiousness in this case are related to the pathogen growth rate and the timing and strength of the specific and non-specific immune responses. Parameters used: k_{pg}, k_m, μ_p, K_{min}, K_{max}, α, x, x_y, k_p, x_n, μ_n, θ, μ_{y_0}, and μ_y.

$U(t) \equiv U(p(t), n(t), y(t))$. This provides some much desired flexibility in defining $\lambda(t)$ since in this host–pathogen system the exact mechanisms by which the immune–pathogen interaction yields disease symptoms are not well understood. Moreover, attempts to define $\lambda(t)$ by explicitly modeling symptoms (not shown) yields qualitatively similar results to those presented here. Note from Eqs. (4.12), (4.14) and the definition of $\lambda(t) = cU(t)$ that if U is linear in a given set of quantities (e.g., p and n), then these relative sensitivities are also linear functions of those quantities since, for any parameter q

$$S_q(\mathbb{P}_s) = -cq \frac{\partial}{\partial q} \left(\int_0^T U(t)\, dt \right). \tag{4.15}$$

Fig. 9A shows the pathogen removal rate $K(y)np$ as an example proxy for symptoms. Other more biologically plausible proxies include defining mortality risk λ as some linear combination of n, p and np. As alluded to earlier in this section, Eq. (4.15) implies that the parameter ranks—as determined by their corresponding sensitivities—are independent of c. It therefore suffices to consider these parameter ranks assuming $\lambda(t)$ is proportional to each of these terms individually, for the two instances of Model (3.1) shown in Fig. 8A. Fig. 9B shows the associated survival probabilities $\mathbb{P}_s$ scale with c exponentially, as expected. Figs. 9C and D show relative sensitivities associated with each of these possible terms used to define $\lambda(t)$. Because $S_q(\mathbb{P}_s)$ is linear if $\lambda(t)$ is linear, one can write the sensitivities for any such $\lambda(t)$ as a linear combination of these values. These results all suggest that host characteristics affecting the timing and strength of the immune response (i.e., μ_n, x, K_{max}, K_{min}, μ_y and μ_{y0}) may respond to disease-induced selection as would host characteristics that affect the pathogen growth rate k_{pg}.

From the perspective of the pathogen, the immune–pathogen dynamics lead to a natural transmission-virulence tradeoff as illustrated in Fig. 10. Assuming variation only in the pathogen growth rate k_{pg} and using the "acute" immune–pathogen dynamics shown in Figs. 8 and 9, the average relationship between transmission and virulence can be computed as shown in Fig. 10.

These results highlight two key aspects of this system. For host and pathogen, the evolutionary consequences of transmission-mediated and/or host-mortality-mediated selection may depend heavily on whether transmission and mortality typically occur before or after the action of the specific immune response (cf. Osnas and Dobson, 2010). This fact likely applies to other persistent or chronic diseases beyond those caused by mycoplasmas. Second, any symptoms-driven selective forces acting on the host could affect both the effectiveness and the timing of the specific immune response as well as the effectiveness of the non-specific response. Since host symptoms are at least partially driven by host immune activity, the direction of selection on host immune characteristics will likely be determined by their net impact on survival.

5. Discussion

One goal of this investigation is to identify which host and pathogen characteristics contribute most to within and between host species variation in disease progression using a simple model of the pathogen–immune interaction. This model exhibits four qualitatively different outcomes of infection with respect to pathogen dynamics: (1) no pathogen proliferation due to effective baseline immune defenses or a relatively low pathogen growth rate, (2) a brief increase in pathogen density allowed by ineffective baseline defenses then clearance by the non-specific immune response, (3) a more prolonged period of pathogen proliferation (resulting from an ineffective non-specific response) that is eventually cleared by the specific immune response, and (4) long-term pathogen persistence despite a sustained specific immune response.
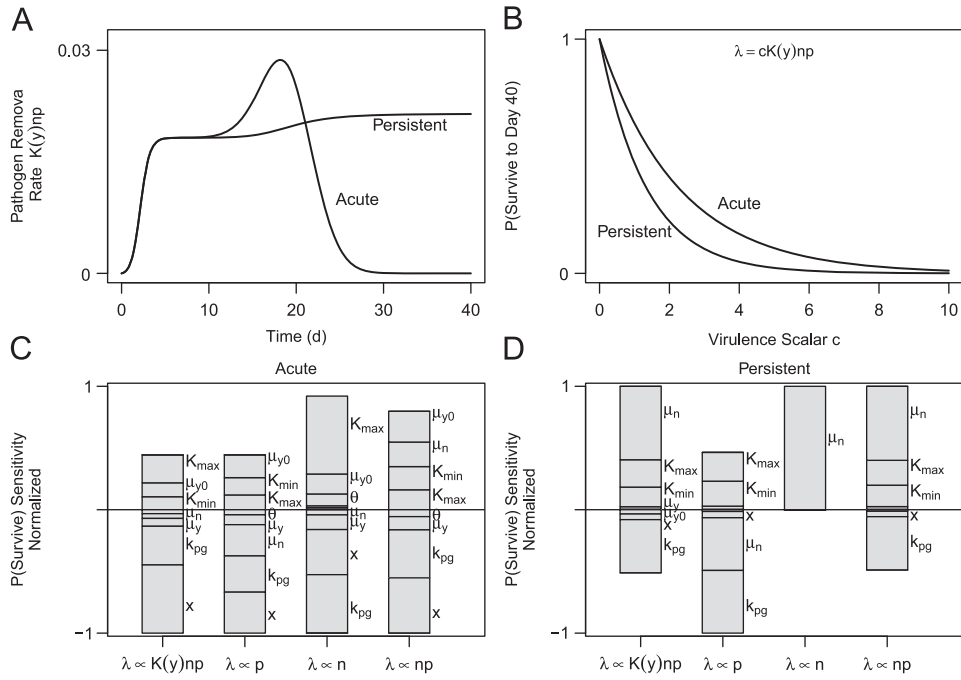
Fig. 9. Sensitivities for the probability of surviving to day 40, $\mathbb{P}_s$, under Model (3.1) showing how host survival responds to small changes in parameter values for the same two cases used in Fig. 8A. Panel A shows one measure of immune-pathogen activity (pathogen removal rate $K(y)np$). Another more general proxy for symptom severity is to define $\lambda(t)$ as a linear combination of p, n and np, as mentioned in the text. Panel B shows how $\mathbb{P}_s$ depends on scaling constant c where $\lambda(t) = cK(y)np$. Panels C and D show approximate parameter sensitivities that have been normalized for each choice of $\lambda(t)$ and plotted as sorted stacked barplots since these normalized relative sensitivities are independant of c (see text). Any choice of $\lambda(t)$ that is a linear combination of these quantities will yield sensitivities that are a linear combination of the normalized sensitivities shown, as detailed in the text. Parameters with sensitivities that are approximately 0 are not labeled. Parameters used: k_{pg}, k_m, μ_p, K_{min}, K_{max}, α, x, x_y, k_p, x_n, μ_n, θ, μ_{y_0}, and μ_y.
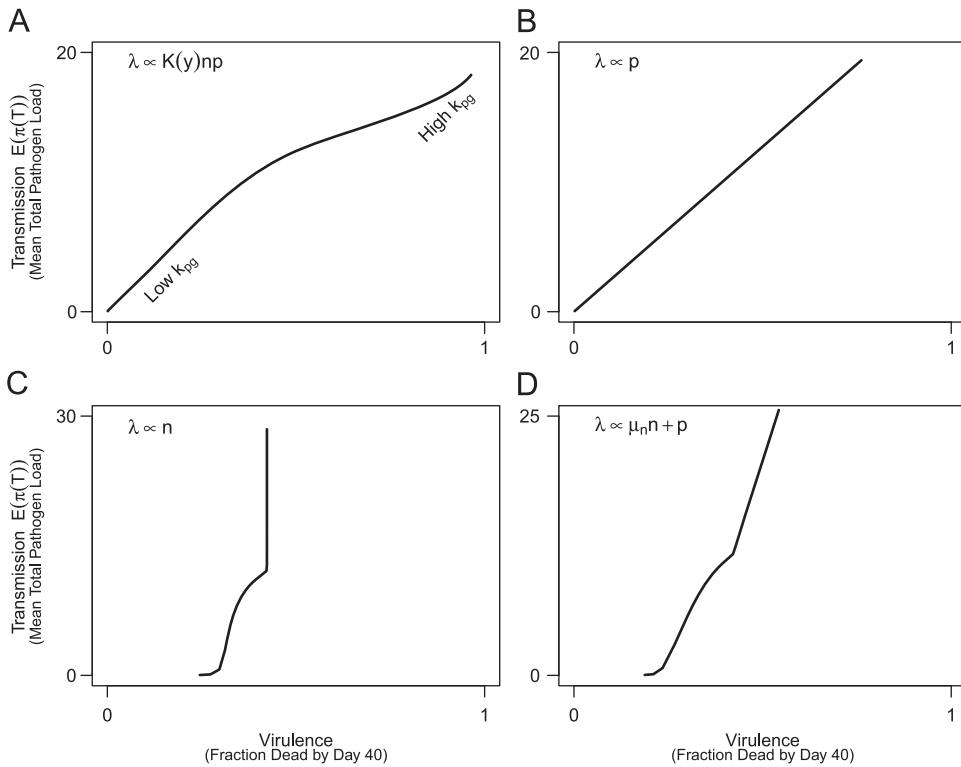

Fig. 10. Transmission–virulence relationships arising from variation in the pathogen growth rate k_{pg}, using different proxies for disease-related mortality risk $\lambda(t)$ as described in Fig. 9 and the text. These positive relationships indicates the existence of a transmission–virulence tradeoff for the pathogen. Here k_{pg} increases from 10% to 10-times of the value given in Table 1. For each value of k_{pg}, the distribution given by Eq. (4.12) was used to compute $E(\pi(T))$ and $\mathbb{P}_s$ (see Fig. 9 and the text). Parameter c was chosen to yield $\mathbb{P}_s = 60\%$ for the value of k_{pg} given in Table 1.

These results suggest that key determinants of these different infection outcomes include the pathogen growth rate (k_{pg}) relative to the host's baseline immune defenses, the ability of non-specific and specific immune components to remove pathogen, and other host characteristics affecting the activation and maintenance of various immune components.

Fig. 11 compares the data shown in Fig. 1 with model output generated by varying three parameters that most affect pathogen load early during infection (see Appendix E for similar figures using other parameters). This suggests that much of the variation between infections in house finches likely results from non-specific immune components (e.g., macrophages) that are variously unable to control *M. gallisepticum* (MG) infections, and perhaps from a delayed or mildly inefficient specific immune response. Importantly, variation in the timing of the specific immune response could also be caused by non-specific immune components involved in activating and regulating the specific immune response. Another important source of variation between species is the pathogen growth rate, which may be species-specific, may differ between strains of MG, and may be influenced by environmental mediators such as temperature. The role of the non-specific immune response in this model is consistent with what is known about other mycoplasma diseases, suggesting that the results presented here may also apply to other host–pathogen systems, not just MG in the house finch. For example, the house sparrow (*Passer domesticus*) is know to have a strong non-specific immune response compared to related species (Lee et al., 2005; Lee, 2006; Martin et al., 2004) and clears MG infections rapidly (Dhondt, 2008).

In the model presented here tacitly assumes that different infection outcomes arise from differing host and/or pathogen characteristics. Another interpretation of these results is suggested by how MG and other mycoplasma species interact with their hosts. The outcome of MG infection can be influenced by the nature of the initial contact with pathogen (e.g., Dhondt, 2007b). Some mycoplasmas are known to actively manipulate the host immune response, making it more ineffective and harmful to the host (Citti et al., 2005; Simecka, 2005). Accordingly, an alternative to interpreting different model parameterizations as fixed individual- or species-level characteristics is to view them as characteristics of a single infection that arise from a multitude of factors including the host's attempt to mount an effective specific immune response and the pathogen's attempt to manipulate that response. Future work comparing the results presented here with models that include more detailed immune regulatory mechanisms may suggest experimental means of determining whether or not immune manipulation plays an important role in these systems.

A second goal of this investigation is to identify pathogen and host immune characteristics likely to affect host infectiousness (pathogen fitness) and mortality risk (host fitness) to help inform the empirical study of virulence evolution in this system. According to the sensitivity profiles shown in Fig. 8, the nature of the selective forces acting on the pathogen depends strongly on whether transmission occurs before or after the specific immune response. Assuming transmission typically occurs early during infections, the characteristics that likely drive pathogen fitness are the pathogen growth rate k_{pg} and any ability of the pathogen to manipulate the non-specific immune response (i.e., to reduce K_{min} and K_{max}). A more complete picture of how host fitness is affected by immune status and pathogen load is needed to give reliable predictions regarding selection on host characteristics. However, if host fitness depends on total immune activity as detailed in Section 4.4, one would expect selection to act on characteristics associated with an early and efficient immune response (i.e., non-specific immune components) and immune-driven disease symptoms (e.g., inflammatory mediators).
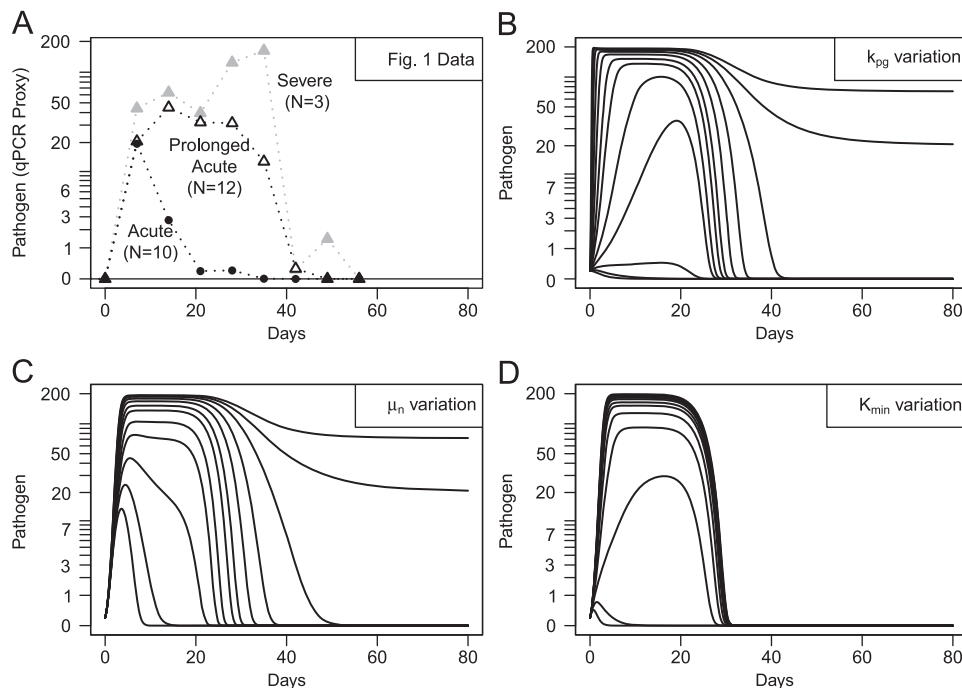

Fig. 11. Comparison between empirically observed pathogen load variation (panel A, from Fig. 1D), and pathogen load variation under Model (3.1) arising from either variation in pathogen (B) or host (C,D) characteristics. The pattern of variation in the data (A) appears more similar to some patterns of host variation (e.g., C) than it does to the pattern arising from pathogen growth rate variation (B). This is consistent with host heterogeneity being an important source of variation in this system. Moreover, these comparisons suggests that the bulk of the observed variation involves the hosts' non-specific immune response. Each parameter shown varies from 5% to 700% of the value given in Table 1, with $K_{min} = 1.2 \times 10^{-3}$, $K_{max} = 2.25 \times 10^{-2}$, $\mu_{y0} = 1.5 \times 10^{-3}$ (to better match the timing of the specific response) and pathogen density p scaled by 200 for plotting model output on the same log-scale as the data. See Fig. E1 in Appendix E for similar figures where other parameters are varied.

This work suggests that certain molecular and cellular level data should help clarify the relationships between mycoplasma, host epithelial tissues, host immune cells and the symptoms associated with MG infection in house finches. Specifically, data from cytokine assays, immune manipulation experiments and data obtained from tissue cultures are likely to shed light on the regulation of various immune components and inflammation, and how MG affects these regulatory processes in avian hosts. Similar data are also needed to establish whether disease symptoms (i.e., tissue inflammation) affect pathogen replication rates and longevity, as such feedbacks might affect the results obtained under Model (3.1). Using mechanistic models such as these to incorporate molecular-, cellular- and organism-level data should clarify our understanding of the complex interactions between mycoplasmas and their hosts.

Appendix A. Scaling the model

The unscaled model is based upon the house finch immune response to MG as described in the text. The resulting non-specific immune model subsystem parallels the non-specific immune model subsystem described in (Reynolds et al., 2006). Therefore the model presented here builds upon that work which is here extended it to include the specific immune response to MG. The unscaled model is given by

$$\frac{dP}{dt} = k_{pg}P\left(1 - \frac{P}{p_\infty}\right) - \frac{k_{pm}s_mP}{\mu_m + k_{mp}P} - K(Y)cNP \tag{A.1a}$$

$$\frac{dN}{dt} = \frac{s_{nr}c(k_{nn}N + k_{np}P)}{\mu_{nr} + c(k_{nn}N + k_{np}P)} - \mu_n N \tag{A.1b}$$

$$\frac{dY_0}{dt} = \frac{k_{ynp}(cNP)^\alpha}{x_{np}^\alpha + (cNP)^\alpha} - \mu_{y0}Y_0 \tag{A.1c}$$

$$\frac{dY}{dt} = \mu_{y0}Y_0 - \mu_y Y \tag{A.1d}$$

where $K(Y) = \left(k_{pn0} + (k_{pnmax} - k_{pn0})Y^\theta / x_{ny}^\theta + Y^\theta\right)$. Model (3.1) in the text is obtained by making the following transformation: $p = P/p_\infty$, $n = N/s_{nr}$, $y_0 = Y_0/k_{ynp}$, $y = Y/k_{ynp}$, $k_{pg} = k_{pg}$, $k_m = k_{pm}s_m/(k_{mp}p_\infty)$, $\mu_p = \mu_m/(k_{mp}p_\infty)$, $K_{min} = cs_{nr}k_{ny0}$, $K_{max} = cs_{nr}k_{np_{max}}$, $\theta = \theta$, $x = x_{ny}/k_{ynp}$, $x_y = x_{np}/(cs_{nr}p_\infty)$, $k_p = k_{np}p_\infty/(k_{nn}s_{nr})$, $x_n = \mu_{nr}/(ck_{nn}s_{nr})$, $\mu_n = \mu_n$, $\alpha = \alpha$, $\mu_{y0} = \mu_{y0}$, $\mu_y = \mu_y$ and time $t = t$.

A.1. Changes from the model in Reynolds et al. (2006)

1. The constant k_{pn} is replaced by the function $K_{pn}(Y_a)$. According to Blanchard and Browning (2005, p. 490) in some species of mycoplasma antibodies are necessary for phagocytosis by innate immune components (e.g. macrophages) so we assume the efficiency of pathogen removal k_{pn} is instead a function of specific immune activity Y and is relatively low without assistance from the specific immune system (at low Y).
2. The anti-inflammatory mediators C_A modeled in Reynolds et al. (2006) are here assumed to be constant, and have been combined with parameter c_∞ into the single parameter $c = 1/1 + (C_a/c_\infty)^2$.
3. To model maturing and active specific immune components (e.g. B- or T-cells, antibodies, etc.) two new state variables were introduced: Y_0 and Y, respectively. Assuming activation and maturation occur in response to antigen presentation by

Table A1
Parameter values of the unscaled model. Time units are hours. Parameters that differ from Table 1 of Reynolds et al. (2006) were assigned values based on their biological interpretation, basic cellular biology of mycoplasmas or to yield biologically plausible dynamics.

Parameter	Value	Range	Description
k_{pg}	0.10	< 2.44	Pathogen growth rate (Reynolds et al., 2006; Flindt and Solomon, 2010; Blanchard and Browning, 2005; Cecchini et al., 2007)
p_∞	2×10^7	$< 1 \times 10^9$	Maximum pathogen density (Reynolds et al., 2006; Flindt and Solomon, 2010)
k_{pm}	0.6	–	Maximum removal by local innate components (Reynolds et al., 2006)
s_m	0.005	≤ 0.005	Influx of local innate components; likely no faster than in (Reynolds et al., 2006)
k_{mp}	0.01	–	Maximum removal by local innate components (Reynolds et al., 2006)
μ_m	0.002	0.0013–0.0048	Decay rate of local innate components (Reynolds et al., 2006)
k_{pn0}	0	$k_{pn0} < k_{pnmax}$	$K(0)$; Pathogen removal rate by active innate components
$k_{pn_{max}}$	1.8	2.5	Maximum pathogen removal rate (Reynolds et al., 2006)
x_{ny}	1	–	Half-saturation constant for $K(Y)$
c	0.75	0–1	Anti-inflammatory mediator effect (held constant) (Reynolds et al., 2006)
s_{nr}	0.08	–	Recruitment of innate components (e.g. phagocytes) (Reynolds et al., 2006)
k_{np}	0.1	–	Pathogen activation of the innate response (Reynolds et al., 2006)
k_{nn}	0.01	≤ 0.1	Positive feedback in the activation of the innate response; no stronger than in Reynolds et al. (2006)
μ_{nr}	0.12	0.069–0.12	Decay rate of baseline innate components (Reynolds et al., 2006)
μ_n	0.05	$\mu_n < \mu_{nr}$	Decay rate of activated innate components (Reynolds et al., 2006)
k_{ynp}	0.005	–	Maximum activation rate of specific immune components
θ	6	≥ 1	Determines steepness of sigmoidal response $K(Y)$ at $Y = x_{ny}$
α	6	≥ 1	Determines steepness of sigmoidal N-activation rate
x_{np}	10	–	Specific component half-saturation constant for activation
μ_{y0}	0.0037	0.003–0.006	Activation rate of specific components; based on a 7–14 day lag
μ_y	0.0016	0.001–0.002	Decay rate of specific components; based on a 7–14 day lag

macrophages the activation rate of the maturing components Y_0 is assumed to be an increasing function of both P and N, with the presence of pathogen and an activated specific immune response required for activation.

Other possibilities for the first term in Eq. (3.1)c include (1) to assume that antigen presentation is more directly related to N levels and that it saturates at low antigen levels (low P), e.g. $k_{ynp}P^\alpha/x_{np}^\alpha + P^\alpha N$; or (2) to assume that it depends on the amount of antigen processed by N, i.e. that the activation rate is proportional to the net rate of pathogen loss $K(Y)NP$.

4. Setting $k_{nd} = 0$ decouples the feedback of damage D to activate innate components (N) by assuming it is negligible w.r.t. the pathogen and self-activation. This assumption removes D from the system simplifying the model mathematically, and it is biologically reasonable as typically *M. gallisepticum* does not seem to lead to self-sustained inflammation.

Appendix B. Simplifying Model (3.1)

The simplified models in the text were derived based on the existence of multiple timescales in the full model and the role certain terms played in driving the dynamics under specific circumstances as explained in the text. Additional details regarding these simplified models are as follows:

1. We assume the p–n subsystem is fast relative to the y_0–y dynamics, and that the n dynamics are fast relative to the p dynamics. In the limit where n tracks p instantaneously, n will approximately satisfy $dn/dt = 0$. Solving for n as a function of p, $n(p)$ is one of the two non-zero roots of dn/dt,

$$n_\pm(p) = \frac{1}{2}\left(\frac{1}{\mu_n} - x_n - k_p p\right) \pm \frac{1}{2}\sqrt{\left(\frac{1}{\mu_n} - x_n - k_p p\right)^2 + 4\frac{1}{\mu_n}k_p p}. \tag{B.1}$$

Requiring $n(p) > 0$ when $p > 0$ and that $n(0) = 0$ implies that we only need consider the case where $n(p) = n_+(p)$, and define

$$n(p) = \frac{1}{2}\left(\frac{1}{\mu_n} - x_n - k_p p\right) + \frac{1}{2}\sqrt{\left(\frac{1}{\mu_n} - x_n - k_p p\right)^2 + 4\frac{1}{\mu_n}k_p p}. \tag{B.2}$$

2. Further simplifications can be made by assuming more direct activation of the adaptive/specific immune response (in the context of mean-field equations, this essentially assumes an exponentially distributed time to activation instead of a gamma distributed delay). This model has a single adaptive immune response variable y replacing Eqs. (A.1c) and (A.1d) with the single equation

$$\frac{dy}{dt} = \frac{(np)^\alpha}{x_y^\alpha + (np)^\alpha} - \mu_y y.$$

This system has the same equilibrium conditions as Model (3.1), but may yield different stability conditions.

3. For parameter values near those given in Table A1, additional simplifications can be made by dropping certain terms from Eq. (3.1) since the model terms are approximately

$$\frac{dp}{dt} = 0.1p(1-p) - \frac{1.5 \cdot 10^{-8}p}{1 \cdot 10^{-8} + p} - \left(\frac{0.1086y^6}{200^6 + y^6}\right)np \tag{B.3a}$$

$$\frac{dn}{dt} = \frac{n + 2.5 \cdot 10^9 p}{199 + n + 2.5 \cdot 10^9 p} - 0.05n \tag{B.3b}$$

$$\frac{dy_0}{dt} = \frac{(np)^6}{8.29 \cdot 10^{-36} + (np)^6} - 0.0037y_0 \tag{B.3c}$$

$$\frac{dy}{dt} = 0.0037y_0 - 0.0016y \tag{B.3d}$$

and

$$n(p) = \frac{1}{2}(-179 - 2.5 \cdot 10^9 p)$$
$$\qquad + \frac{1}{2}\sqrt{(-179 - 2.5 \cdot 10^9 p)^2 + 2 \cdot 10^{11} p}. \tag{B.4}$$

This suggests the following simplifications. The activation of the innate response is primarily driven by pathogen load p, as $k_p \gg 1$. Omitting n from the dn/dt equation leaves

$$\frac{dn}{dt} = \frac{p}{\frac{x_n}{k_p} + p} - \mu_n n \tag{B.5}$$

reducing $n(p)$ to

$$n(p) = \frac{1}{\mu_n}\frac{p}{\frac{x_n}{k_p} + p}. \tag{B.6}$$

Combining the above simplifications yields the simplified p–y model (4.7) which approximates the slow time scale dynamics of model (3.1).

Appendix C. Fast p–n model dynamics

Because different processes in Model (3.1) occur over a broad range of time scales, we can analyze the model dynamics using standard separation of time scales techniques. We first consider the dynamics without an active immune response, then consider the "fast" time scale dynamics given by the p–n model. Results similar to those in AppendicesC.1 and C.2 below were previously discussed in Reynolds et al. (2006) for a very similar model.

C.1. Pathogen dynamics without an immune response

Holding the specific and non-specific immune response constant ($n = 0$), the pathogen dynamics follow

$$\frac{dp}{dt} = k_{pg}p(1-p) - \frac{k_m p}{\mu_p + p} \tag{C.1}$$

where the second term captures the host's baseline immune defenses as detailed in the text.

Eq. (C.1) can have one to three equilibria

$$p_o = 0 \tag{C.2a}$$

$$p_{crit} = \frac{1}{2}\left((1-\mu_p) - \sqrt{(1+\mu_p)^2 - \frac{4}{k_{pg}}k_m}\right) \tag{C.2b}$$

$$p_{max} = \frac{1}{2}\left((1-\mu_p) + \sqrt{(1+\mu_p)^2 - \frac{4}{k_{pg}}k_m}\right) \tag{C.2c}$$

corresponding, respectively, to a state of health (stable when $r_0 < 0$; see text), an unstable equilibrium and threshold for the Allee effect (unstable when p_{crit} positive; same as $r_0 < 0$) and an equilibrium state of pathogen persistence (stable when p_s exists in $(0, 1]$).

C.2. Dynamics of the p–n subsystem

Next we consider the dynamics of the "fast" Model (4.3), where the ("slow" time scale) specific immune dynamics are treated as constant. The equilibria for Eq. (4.3) are

$$(p_o, n_o) = (0, 0) \tag{C.3a}$$

$$(p_n, n_n) = \left(0, \frac{1}{\mu_n} - x_n\right) \tag{C.3b}$$

$$(p_*, n_*), \quad p_*, \, n_* > 0 \tag{C.3c}$$

which correspond to a state of health ((C.3a), the origin), a self-sustaining immune response that can persist in the absence of pathogen (C.3b) and one or more equilibria with positive pathogen density (p_*) and immune activity (n_*). Typically there are only one (e.g. $k_m = 0$) or two interior equilibria (although see figure 4). In rare cases, there can be three interior equilibria, two of which arise at relatively low pathogen densities via a saddle-node bifurcation, resulting in bistability. Ranking the three equilibria by pathogen density, the middle equilibrium acts like an Allee threshold (an unstable equilibrium) resulting in bistability between the upper steady state and a lower steady state (or limit cycle) instead of bistability with the origin.

Stability criteria for these equilibria are as follows. The healthy state (C.3a) is locally stable when $r_0 < 0$ and when the host immune response is not self-sustaining $n_n < 0$, where r_0 and n_n are given by Eqs. (4.2) and (C.3b), respectively. The state of pathogen-free persistent inflammation (C.3b) is caused by the positive feedback in the non-specific immune response (n), and is locally stable whenever $n_n > 0$ and pathogen cannot invade that state $r_0 < K_{ny} n_n$.

Stability criteria for interior equilibria (C.3c) and criteria for an Allee effect are best summarized by considering the nullclines of Model (4.3) given by $dp/dt = 0$ and $dn/dt = 0$. The p- and n-nullclines are, respectively

$$n(p) = \frac{\left(k_{pg}(1-p) - \frac{k_m}{\mu_p + p}\right)}{K_{ny}}, \quad p = 0 \tag{C.4a}$$

$$p(n) = \frac{n}{k_p}\left(\frac{x_n}{\frac{1}{\mu_n} - n} - 1\right) \tag{C.4b}$$

For clarification, the p and n nullclines can be regarded as being restricted to the positive quadrant of the p–n plane with p on the horizontal axis and n on the vertical axis, as shown in Fig. 4. We can rewrite the nullclines Appendix (C.4) as functions of p when restricted to the positive quadrant.

$$f_p(p) = \frac{\left(k_{pg}(1-p) - \frac{k_m}{\mu_p + p}\right)}{K_{ny}}, \quad p = 0 \tag{C.5a}$$

$$f_n(p) = \frac{1}{2}\left((n_n - k_p p) + \sqrt{(n_n - k_p p)^2 + \frac{4k_p}{\mu_n}p}\right) \tag{C.5b}$$

The simpler of the two ($f_n(p)$, the n-nullcline) is described first. This curve is concave down and either increases from the origin or ($p=0$, $n=n_n$) toward $n \to \mu_n$ with increasing p (see solid curve in Fig. 4).

If $k_m = 0$ the p-nullcline is simply a decreasing line intersecting the axes at ($p=0$, $n=k_{pg}/K_{ny}$) and ($p=1$, $n=0$). If $k_m > 0$, the second term in (C.4a) introduces a vertical asymptote at $p = -\mu_p$. This makes the p-nullcline concave down and it intersects the p-axis twice: it increases through the p-axis somewhere above $p = -\mu_p$ and decreases across the p-axis between $1 - \mu_p$ and 1. These two roots are given by

$$p_\pm = \frac{1}{2}\left((1 - \mu_p) \pm \sqrt{(1 + \mu_p)^2 - \frac{4}{k_{pg}}k_m}\right) \tag{C.6}$$

The lower root is positive only if $k_m/\mu_p > k_{pg}$ (i.e. when Model (4.1) shows bistability). When (C.4a) is unimodal over the domain (0, 1), the peak occurs at $p = \sqrt{k_m/k_{pg}} - \mu_p$.

Having described these two nullclines in detail, we may now consider the stability criteria of interior equilibrium points.

C.2.1. Stability of Interior Equilibria of (4.3)

On the positive quadrant of the p–n plane under Model (4.3), denote the p-nullcline by $f_p(p)$ and the n-nullcline by $f_n(p)$ according to Eqs. (C.5). Assume these curves intersect to yield an equilibrium point (p_*, n_*). Stability of this equilibrium is determined by the sign of the Jacobian's trace and determinant at this point, where

$$\text{sign}(-Tr) = \text{sign}\left(-pK_{ny}f_p'(p) + \frac{d}{dp}\left[\frac{dn}{dt}\right]\frac{1}{f_n'(p)}\right)_{(p,n)=(p_*,n_*)} \tag{C.7a}$$

$$\text{sign}(Det) = \text{sign}(f_n'(p) - f_p'(p))_{(p,n)=(p_*,n_*)} \tag{C.7b}$$

The stability conditions for (p_*, n_*) can be summarized as

$$f_p'(p) < \min\left(f_n'(p), \frac{d}{dp}\left[\frac{dn}{dt}\right]\frac{1}{pK_{ny}f_n'(p)}\right)_{(p,n)=(p_*,n_*)} \tag{C.8}$$

where loss of stability via a Hopf bifurcation results in

$$\frac{\left(\frac{d}{dp}\left[\frac{dn}{dt}\right]\right)_{(p_*,n_*)}}{p_* K_{ny} f_n'(p_*)} < f_p'(p_*) < f_n'(p_*) \tag{C.9}$$

Limited numerical investigation suggests cycling dynamics in the fast p–n subsystem are rare and of small amplitude for biologically relevant parameter values.

These criteria have the following implications:

1. Here, both $f_n'(p) > 0$ and $d/dp(dn/dt) > 0$ hold. This implies that Hopf bifurcations require both nullclines be increasing functions of p.
2. If the p-nullcline is a strictly decreasing function on all of $p \in (0, 1)$—e.g. if $k_m \approx 0$—there can be no stable limit cycle oscillations. Therefore in this case a necessary (but not sufficient) requirement for cycling is that (i.e., $k_m \geq k_{pg}\mu_p^2$).

C.3. Simplified p–n model dynamics

In the text we simplify the p–n model (4.3) by omitting positive feedback in the activation rate of n. This yields the new form of dn/dt given by Eq. (4.4). Here we detail the dynamics of this simplified p–n model.

First, we rewrite the model equations in terms of their nullclines

$$\frac{dp}{dt} = (f_p(p) - n)K_{ny}p \tag{C.10a}$$

$$\frac{dn}{dt} = (f_n(p) - n)\mu_n \tag{C.10b}$$

where the p-nullcline (for $p > 0$) is $f_p(p)$ (C.5a) and the n-nullcline is $f_n(p) \equiv \mathbf{n}(p)$ (4.5).

The stability of the origin under this model is as stated in the text, with $r_0 > 0$ required for pathogen invasion. Linearizing this system about any equilibrium with $p_* > 0$, $n_* > 0$ yields a Jacobian matrix with trace and determinant

$$-Tr = -p_* K_{ny} f_p'(p_*) + \mu_n \tag{C.11a}$$

$$Det = \mu_n K_{ny} p_*(f_n'(p_*) - f_p'(p_*)). \tag{C.11b}$$

This equilibrium is stable when these two quantities are positive with loss of stability via a Hopf bifurcation when Tr increases through 0.
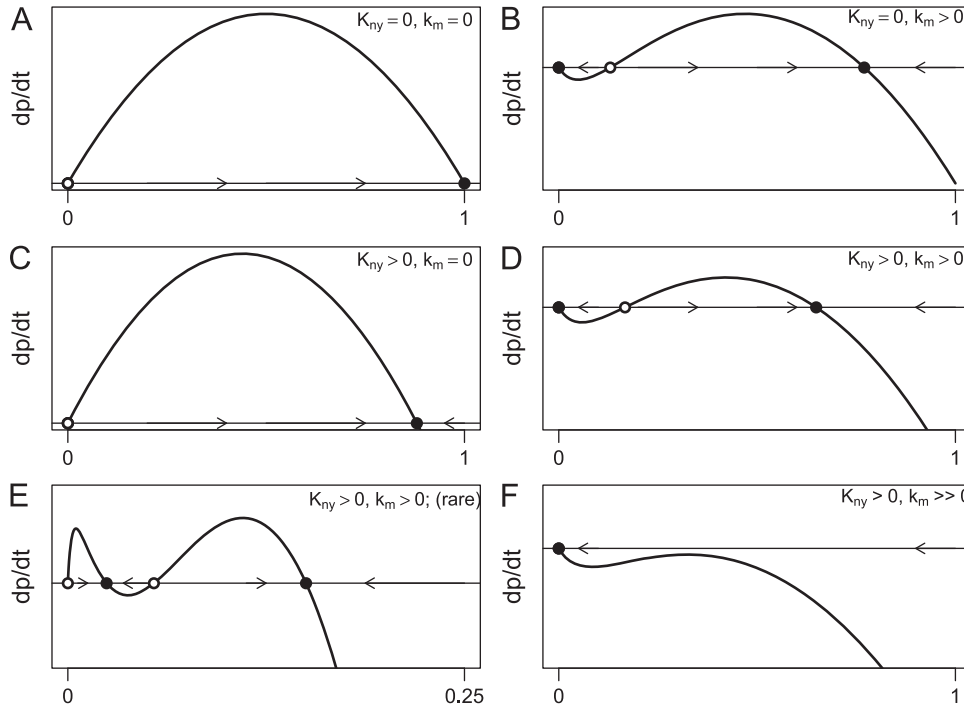
Fig. C1. Dynamics of Model (4.6) which approximate the simplified p–n subsystem when n-dynamics are fast.

C.4. Pathogen dynamics with fast n

Assuming a fast non-specific response (n) under the simplified p–n model given by Equations (4.3a) and (4.4), we can approximate that subsystem with the single equation (4.6). Relative to the simplified p–n model, the dynamics of (4.6) can be summarized as follows (see Fig. C1).

The equilibria of the simplified p–n model satisfy $dp/dt = 0$ and $dn/dt = 0$, and therefore those equilibrium pathogen densities are exactly the equilibria of the one dimensional model (4.6). Writing Eq. (4.6) using the p and n nullclines in the previous section

$$\frac{dp}{dt} = (f_p(p) - f_n(p)) K_{ny} p. \tag{C.12}$$

Linearizing about an equilibrium point $p_* > 0$ gives the stability condition

$$f'_n(p_*) - f'_p(p_*) > 0. \tag{C.13}$$

Recalling stability conditions (C.11), it follows that if $p_*, n_* > 0$ is stable under the simplified p–n model then p_* is necessarily a stable equilibrium of the one dimensional model (4.6). Likewise, unstable equilibria associated with stable limit cycles will be stable under Model (4.6) so long as (C.11b) remains positive.

Appendix D. Slow p–y model dynamics

We here rewrite the p–y model equations (4.7) in a more general form

$$\frac{dp}{dt} = \left(k_{pg}(1-p) - \frac{k_m}{\mu_p + p} - K(y)\mathbf{n}(p) \right) p \tag{D.1a}$$

$$\frac{dy}{dt} = G(p) - \mu_y y. \tag{D.1b}$$

where $G(p)$ is the specific immune activation rate, $G(p) = (\mathbf{n}(p)p)^\alpha / ((\mathbf{n}(p)p)^\alpha + x_y^\alpha)$. More generally the results below hold for other choices of G where $G(0) = G'(0) = 0$, $G'(p) \geq 0$ and $G(p) \leq G_{max}$.

The equilibria of the p–y model (4.7) are only the origin (the healthy state) and the intersections of the nullclines (4.9) in the interior of the positive quadrant, since $\mathbf{n}(0) = 0$ (i.e. there is no self-sustaining inflammatory response). Stability conditions for these equilibria are as follows:

The origin has eigenvalues $\lambda_1 = r_0$ and $\lambda_2 = -\mu_y$, where r_0 is given by (4.2) and hence local stability is determined by whether r_0 is greater or less than 0.

Stability of the interior equilibria can be considered first under the simple case where $k_m = 0$. An interior equilibrium point is stable when the Jacobian's determinant is positive and its trace negative. For Model (D.1),

$$-Tr(J) = \mu_y + (k_{pg} + K(y)\mathbf{n}'(p))p \tag{D.2a}$$

$$Det(J) = ((k_{pg} + K(y)\mathbf{n}'(p))\mu_y + K'(y)\mathbf{n}(p)G'(p))p. \tag{D.2b}$$

Recalling that $\mathbf{n}(p)$, $K(y)$ and $G(p)$ are each increasing functions, stability is ensured as both of the quantities above are positive for any equilibrium quantities p, $y > 0$.

More generally, if $k_m > 0$ then

$$-Tr(J) = \mu_y + \left(k_{pg} + K(y)\mathbf{n}'(p) - \frac{k_m}{(\mu_p + p)^2} \right) p \tag{D.3a}$$

$$Det(J) = \left(\left(k_{pg} + K(y)\mathbf{n}'(p) - \frac{k_m}{(\mu_p + p)^2} \right) \mu_y + K'(y)\mathbf{n}(p)G'(p) \right) p \tag{D.3b}$$

Here stability can be lost if either of these two quantities becomes negative. The loss of stability via a Hopf bifurcation occurs when (D.3a) passes through 0. Computational results suggest that cycling dynamics only occur rarely and with small amplitudes for parameter values relevant to this particular biological application. They occur during instances of bi- or multi-stability and typically have small basins of attraction. That said, they may have some relevance to the loss of low-level pathogen persistence via stochastic extinction.

D.1. Nullclines of the p–y model

The nullclines of the p–y model (D.1a,b) for positive values p and y are

$$g_p(p) = K^{-1} \left(\frac{k_{pg}(1-p) - \dfrac{k_m}{\mu_p + p}}{\mathbf{n}(p)} \right) \quad \text{(D.4a)}$$

$$g_y(p) = \frac{G(p)}{\mu_y} \quad \text{(D.4b)}$$

For the case of $G(p)$ considered in the text, the y-nullcline (4.9b) is a strictly increasing function of p, increasing from the origin and asymptotically approaching the saturating value $y = \mu_y^{-1}$. The y-nullcline reaches half that maximum value when $p = p_{1/2}$

defined by $\mathbf{n}(p_{1/2})p_{1/2} = x_y$ (see Eq. (4.9b)) and given explicitly by

$$p_{1/2} = x_y \mu_n \left(\frac{1 + \sqrt{1 + 4\dfrac{x_n/k_p}{x_y \mu_n}}}{2} \right) \quad \text{(D.5)}$$

Recall from the full Model (3.1) that the activation rates of the innate (n) and specific (y_0) immune responses (see the first terms in (3.1b,c)) reach half of their maximum value when $p = x_n/k_p$ and $p = x_y$, respectively. If the innate response reaches a maximum activity level at relatively small p (i.e. $k_p/x_n \gg 1$), then $\mathbf{n}(p)$ is approximately its upper limit of $1/\mu_p$ for most $p \in (0,1)$. If $x_n/k_p \ll x_y \mu_n$, then $p_{1/2} \approx x_y \mu_n$. If $x_n/k_p \gg x_y \mu_n$ then $p_{1/2} \approx \sqrt{x_y \mu_p x_n/k_p}$.
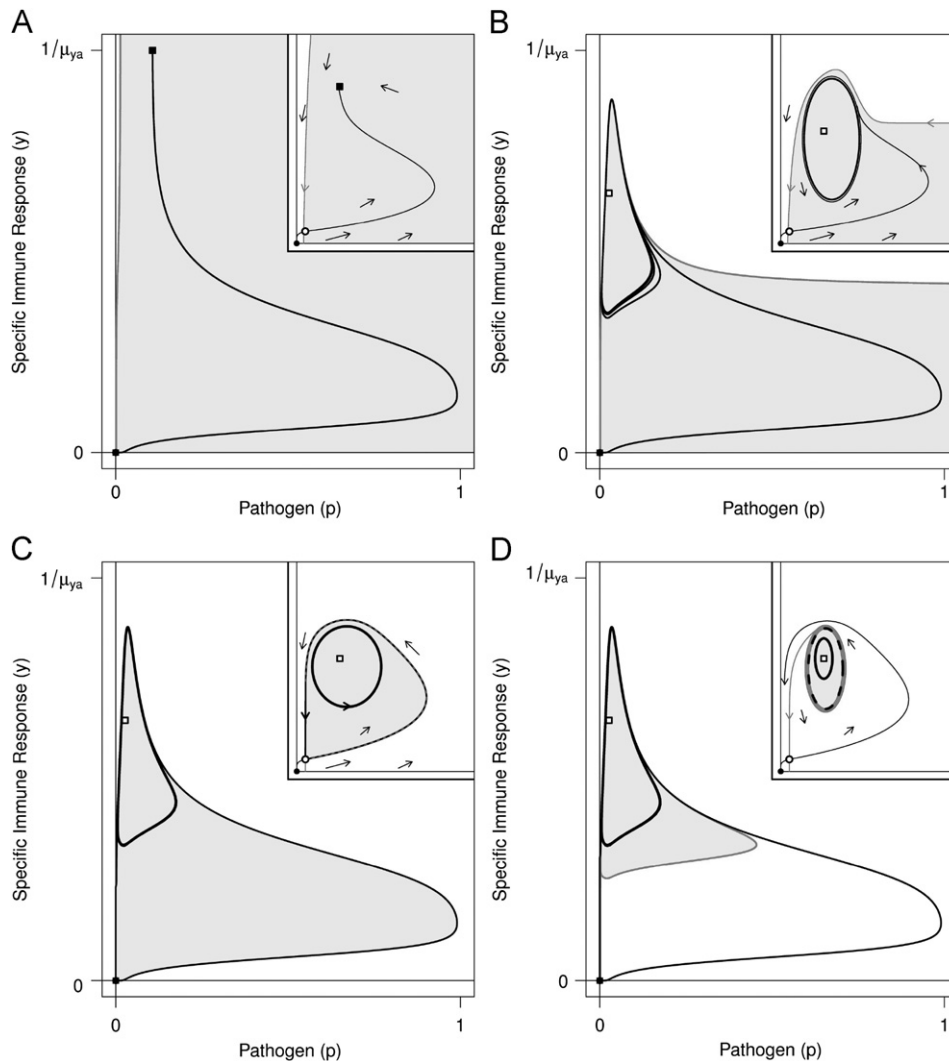

Fig. D1. Details of the transition indicated by the arrow in Fig. 5B for the p–y model (4.7) parameterized to exhibit bistability. Topologically equivalent insets are included for clarification and to show the unstable saddle (empty circle in the inset) that is so near the origin that the solid (origin) and empty (saddle) circles overlap. This transition can be understood as the result of a saddle homoclinic bifurcation near a generalized Hopf bifurcation. This figure shows the p–y dynamics before (Panels A, B), at (Panel C) and after (Panel D) the saddle homoclinic. Shading indicates the basin of attraction for disease persistence, non-shaded regions lead to the origin and the boundary between basins of attraction is the stable manifold of a saddle equilibrium (empty circle in the insets). Panel A: Starting at low K_{max}, infections lead to a state of pathogen persistence. Panel B: Increasing K_{max} through the transition region, the boundary between basins of attraction bends away from the y axis increasing the origin's basin of attraction. For most parameter sets considered, the persistence equilibrium undergoes a Hopf bifurcation resulting in cycling dynamics at low pathogen density, as shown. Panel C: At the saddle homoclinic bifurcation, a homoclinic orbit is formed as the stable and unstable manifolds of the saddle connect as shown in the inset. This gives rise to an unstable limit cycle that contains the basin of attraction for pathogen persistence. Panel D: Beyond this bifurcation, nearly all biologically meaningful trajectories lead to the origin, most after a brief excursion that corresponds to an acute infection resolved by the host immune response. See text for additional details.

Letting $F(p) = (k_{pg}(1-p) - k_m/\mu_p + p)/\mathbf{n}(p)$, the slope of the null-clines (D.4) at an equilibrium point (p_*, y_*) are, respectively

$$g'_p(p_*) = K^{-1'}(F(p_*))F'(p_*) \qquad \text{(D.6a)}$$

$$g_y'(p_*) = \frac{G'(p_*)}{\mu_y} \qquad \text{(D.6b)}$$

where the signs of $K^{-1'}(\cdot)$ and $G'(\cdot)$ are positive and the sign of $F'(\cdot)$ may be positive or negative, since at any positive valued equilibrium point (p,y)

$$F'(p) = -\left(k_{pg} + K(y)\mathbf{n}'(p) - \frac{k_m}{(\mu_p + p)^2}\right)\frac{1}{\mathbf{n}(p)}.$$

To relate the slope of the nullclines to the stability criteria (D.3), a little calculus gives that $K^{-1'}(F(p_*)) = 1/K'(y_*)$ and hence $g'_p(p_*) = F'(p_*)/K'(y_*)$. Together with (D.6a) this yields the general ($k_m \geq 0$) stability criteria

$$-Tr(J) = \mu_y - g'_p(p_*)K'(y_*)\mathbf{n}(p_*)p_* \qquad \text{(D.7a)}$$

$$Det(J) = (g_y'(p_*) - g'_p(p_*))K'(y_*)\mathbf{n}(p_*)p_*\mu_y \qquad \text{(D.7b)}$$

Since the p-nullcline increases and decreases where $F(p)$ increases and decreases, respectively, the Hopf condition (D.7a) shows that the only equilibria that can undergo a Hopf bifurcation are those that occur where the p-nullcline is increasing with a large enough slope s.t. $g'_p(p_*) > \mu_y/K'(y_*)\mathbf{n}(p_*)p_*$.

D.2. The transition from persistence to clearance

The bifurcations involved in the transition from low-level pathogen persistence to pathogen clearance indicated with an arrow in Fig. (5) are illustrated in Fig. D1B where K_{max} is increased through a very narrow region of parameter space. To better illustrate key details, insets are included in Fig. D1 that contain topologically equivalent illustrations of the dynamics. We are particularly interested in initial conditions that correspond to a newly infected naive host, i.e. initial conditions that lie along the p-axis with very low pathogen density.

Preceding the transition (low K_{max}, see Fig. D1A), the basin of attraction for the persistence steady state (shaded gray) is large while the basin of attraction for the healthy state (shaded white) is a very small region near $p \approx 0$. As show in the inset, there is a saddle equilibrium near the origin whose stable manifold forms the boundary between initial conditions that lead to the origin or to (p_*, n_*). Increasing K_{max} very near the transition zone (see Fig. D1B), it is also possible (though not necessary) for the persistence steady state to undergo a supercritical Hopf bifurcation resulting in pathogen–immune cycles. Next there is an abrupt change in the two basins of attraction that appear to result from a homoclinic bifurcation (Fig. D1C). As K_{max} increases through this bifurcation, the arm of stable manifold (dark gray curve) separating the two regions lifts off of the y axis (Fig. D1A to B) and wraps around a neighborhood of the persistence steady state (or cycle) eventually intersecting the p axis. Continuing, this
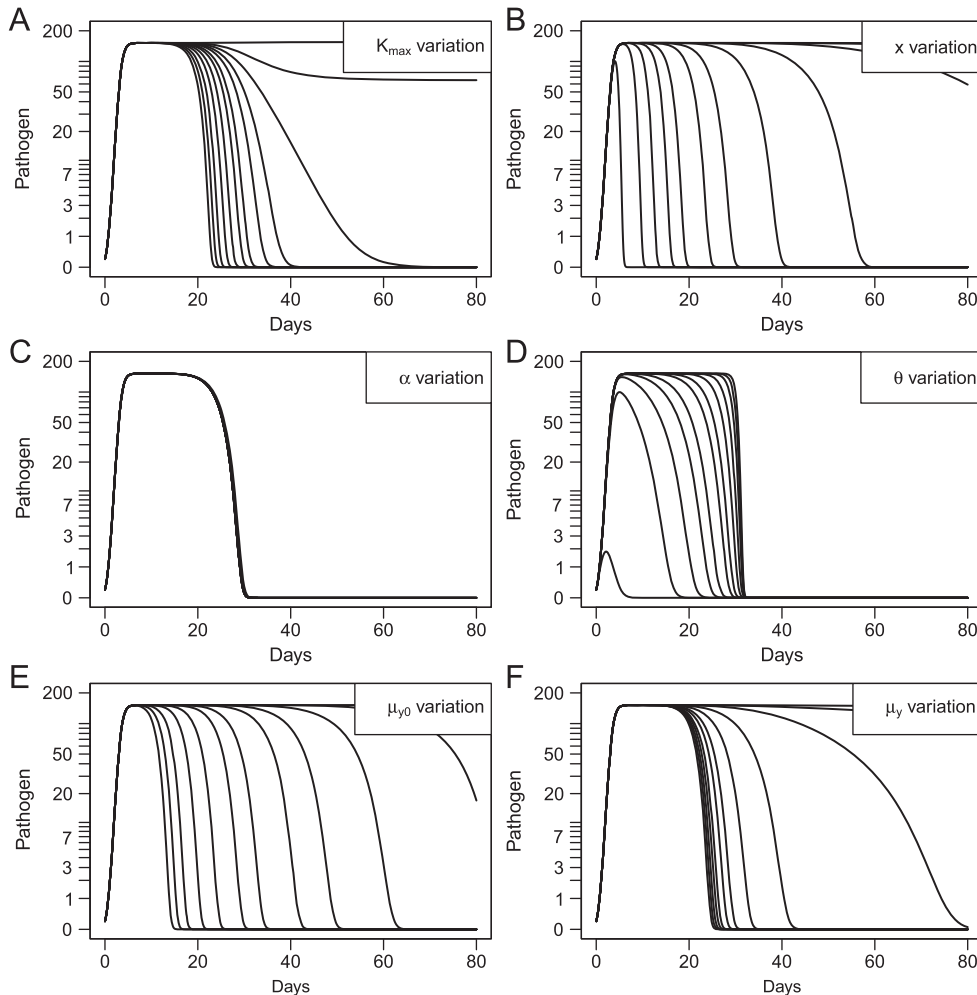

Fig. E1. Pathogen load variation under Model (3.1). See Fig. 11 for details.

motion, it eventually intersects the unstable manifold of the saddle and forms a homoclinic orbit like the one shown in the Fig. D1C inset. Beyond this point, an unstable limit cycle is born from the homoclinic bifurcation and the stable manifold now spirals backwards onto this cycle leaving the interior of that cycle as the basin of attraction for disease persistence (either cycling or at steady state). Note that now all initial conditions of the form $(p > 0, y = 0)$ yield either no infection ($p \approx 0$) or an acute infection resolved by the specific immune response. Increasing K_{max} further, the region yielding disease persistence continues to shrink and may disappear via either a saddle-node of limit cycles or a subcritical Hopf bifurcation when the unstable limit cycle collides with the stable limit cycle or stable persistence equilibrium, respectively.

Appendix E. Parameter variation and sensitivity analysis

References

Aldrich, J.W., Weske, J.S., 1978. Origin and evolution of the eastern house finch population. Auk 95 (3), 528–536.

Altizer, S., Hochachka, W.M., Dhondt, A.A., 2004a. Seasonal dynamics of mycoplasmal conjunctivitis in eastern north american house finches. J. Anim. Ecol. 73 (2), 309–322.

Altizer, S., Davis, A.K., Cook, K.C., Cherry, J.J., 2004b. Age, sex, and season affect the risk of mycoplasmal conjunctivitis in a southeastern house finch population. Can. J. Zool. 82 (5), 755–763, http://dx.doi.org/10.1139/Z04-050.

Altizer, S., Dobson, A., Hosseini, P., Hudson, P., Pascual, M., Rohani, P., 2006. Seasonality and the dynamics of infectious diseases. Ecol. Lett. 9 (4), 467–484, http://dx.doi.org/10.1111/j.1461-0248.2005.00879.x.

Baseman, J.B., Tully, J.G., 1997. Mycoplasmas: sophisticated, reemerging, and burdened by their notoriety. Emerg. Infect. Dis. 3 (1), 21–32, http://dx.doi.org/10.3201/eid0301.970103.

Blanchard, A., Browning, G. (Eds.), 2005. Mycoplasmas: Molecular Biology Pathogenicity and Strategies for Control. Horizon Bioscience, Wymondham, Norfolk, U.K.

Brown, D.R., Zacher, L.A., Wendland, L.D., Brown, M.B., 2005. Emerging mycoplasmoses in wildlife. In: Blanchard, A., Browning, G. (Eds.), Mycoplasmas Molecular Biology Pathogenicity and Strategies for Control. Horizon Bioscience, Wymondham, Norfolk, U.K, pp. 383–414. (Chapter 11).

Brown, D.R., Whitcomb, R.F., Bradbury, J.M., 2007. Revised minimal standards for description of new species of the class Mollicutes (division Tenericutes). Int. J. Syst. Evol. Microbiol. 57 (11), 2703–2719, http://dx.doi.org/10.1099/ijs.0.64722-0.

Cecchini, K.R., Gorton, T.S., Geary, S.J., 2007. Transcriptional responses of Mycoplasma gallisepticum strain R in association with eukaryotic cells. J. Bacteriol. 189 (16), 5803–5807, http://dx.doi.org/10.1128/JB.00667-07.

Cherry, J.J., Ley, D.H., Altizer, S., 2006. Genotypic analyses of Mycoplasma gallisepticum isolates from songbirds by random amplification of polymorphic DNA and amplified-fragment length polymorphism. J. Wildl. Dis. 42 (2), 421–428.

Citti, C., Browning, G.F., Rosengarten, R., 2005. Phenotypic diversity and cell invasion in host subversion by pathogenic mycoplasmas. In: Blanchard, A., Browning, G. (Eds.), Mycoplasmas: Molecular Biology Pathogenicity and Strategies for Control. Horizon Bioscience, Wymondham, Norfolk, U.K., pp. 439–483. (Chapter 13).

Cooper, C.B., Hochachka, W.M., Dhondt, A.A., 2007. Contrasting natural experiments confirm competition between house finches and house sparrows. Ecology 88 (4), 864–870, http://dx.doi.org/10.1890/06-0855.

Dhondt, A., Tessaglia, D., Slothower, R., 1998. Epidemic mycoplasmal conjunctivitis in house finches from eastern North America. J. Wildl. Dis. 34 (2), 265–280.

Dhondt, A., Badyaev, A., Dobson, A., Hawley, D., Driscoll, M., Hochachka, W., Ley, D., 2006. Dynamics of mycoplasmal conjunctivitis in the native and introduced range of the host. EcoHealth 3, 95–102, http://dx.doi.org/10.1007/s10393-006-0019-7.

Dhondt, A.A., Altizer, S., Cooch, E.G., Davis, A.K., Dobson, A., Driscoll, M.J., Hartup, B.K., Hawley, D.M., Hochachka, W.M., Hosseini, P.R., Jennelle, C.S., Kollias, G.V., Ley, D.H., Swarthout, E.C., Sydenstricker, K.V., 2005. Dynamics of a novel pathogen in an avian host: mycoplasmal conjunctivitis in house finches. Acta Tropica 94 (1), 77–93, http://dx.doi.org/10.1016/j.actatropica.2005.01.009.

Dhondt, A.A., Dhondt, K.V., Hawley, D.M., Jennelle, C.S., 2007a. Experimental evidence for transmission of Mycoplasma gallisepticum in house finches by fomites. Avian Pathol. 36 (3), 205–208, http://dx.doi.org/10.1080/03079450701286277.

Dhondt, A.A., Dhondt, K.V., McCleery, B.V., 2008. Comparative infectiousness of three passerine bird species after experimental inoculation with Mycoplasma gallisepticum. Avian Pathol. 37 (6), 635–640, http://dx.doi.org/10.1080/03079450802499100.

Dhondt, K.V., Dhondt, A.A., Ley, D.H., 2007b. Effects of route of inoculation on Mycoplasma gallisepticum infection in captive house finches. Avian Pathol. 36 (6), 475–479, http://dx.doi.org/10.1080/03079450701642016.

Edward, D.G.f., Freundt, E.A., 1967. Proposal for Mollicutes as name of the class established for the order Mycoplasmatales. Int. J. Syst. Bacteriol. 17 (3), 267–268, http://dx.doi.org/10.1099/00207713-17-3-267.

Edward, D.G.f., Kanarek, E.A., 1960. Organisms of the pleuropneumonia group of avian origin: their classification into species. Ann. N. Y. Acad. Sci. 79 (10), 696–702, http://dx.doi.org/10.1111/j.1749-6632.1960.tb42744.x.

Elliott, J.J., Aribib Jr., R.S., 1953. Origin and status of the eastern house finch in the eastern United States. Auk 70 (1), 31–37.

Farmer, K.L., Hill, G.E., Roberts, S.R., 2005. Susceptibility of wild songbirds to the house finch strain of Mycoplasma Gallisepticum. J. Wildl. Dis. 41 (2), 317–325.

Faustino, C.R., Jennelle, C.S., Connolly, V., Davis, A.K., Swarthout, E.C., Dhondt, A.A., Cooch, E.G., 2004. Mycoplasma gallisepticum infection dynamics in a house finch population: seasonal variation in survival,bb encounter and transmission rate. J. Anim. Ecol. 73 (4), 651–669, http://dx.doi.org/10.1111/j.0021-8790.2004.00840.x.

Fischer, J.R., Stallknecht, D.E., Luttrell, P., Dhondt, A.A., Converse, K.A., 1997. Mycoplasmal conjunctivitis in wild songbirds: the spread of a new contagious disease in a mobile host population. Emerg. Infect. Dis. 3 (1), 69–72, http://dx.doi.org/10.3201/eid0301.970110.

Flindt, R., Solomon, N., 2006. Amazing Numbers in Biology, first ed. Springer Berlin Heidelberghttp://dx.doi.org/10.1007/3-540-30147-X.

Grodio, J.L., Dhondt, K.V., O'Connell, P.H., Schat, K.A., 2008. Detection and quantification of Mycoplasma gallisepticum genome load in conjunctival samples of experimentally infected house finches (Carpodacus mexicanus) using real-time polymerase chain reaction. Avian Pathol. 37 (4), 385–391, http://dx.doi.org/10.1080/03079450802216629.

Grodio, J.L., Hawley, D.M., Osnas, E.E., Ley, D.H., Dhondt, K.V., Dhondt, A.A., Schat, K.A., 2011. Pathogenicity and immunogenicity of three Mycoplasma gallisepticum isolates in house finches (Carpodacus mexicanus). Vet. Microbiol. 155 (1), 53–61, http://dx.doi.org/10.1016/j.vetmic.2011.08.003.

Hartup, B., Mohammed, H., Kollias, G., Dhondt, A., 1998. Risk factors associated with mycoplasmal conjunctivitis in house finches. J. Wildl. Dis. 34 (2), 281–288.

Hartup, B., Dhondt, A., Sydenstricker, K., Hochachka, W., Kollias, G., 2001a. Host range and dynamics of mycoplasmal conjunctivitis among birds in North America. J. Wildl. Dis. 37 (1), 72–81.

Hartup, B.K., Bickal, J.M., Dhondt, A.A., Ley, D.H., Kollias, G.V., 2001b. Dynamics of conjunctivitis and Mycoplasma gallisepticum infections in house finches. Auk 118 (2), 327–333, http://dx.doi.org/10.1642/0004-8038(2001)118[0327: DOCAMG]2.0.CO;2.

Hawley, D.M., Sydenstricker, K.V., Kollias, G.V., Dhondt, A.A., 2005. Genetic diversity predicts pathogen resistance and cell-mediated immunocompetence in house finches. Biol. Lett. 1 (3), 326–329, http://dx.doi.org/10.1098/rsbl.2005.0303.

Hawley, D.M., Lindström, K., Wikelski, M., 2005a. Experimentally increased social competition compromises humoral immune responses in house finches. Horm. Behav. 49 (4), 417–424, http://dx.doi.org/10.1016/j.yhbeh.2005.09.003.

Hawley, D.M., Hanley, D., Dhondt, A.A., Lovette, I.J., 2006. Molecular evidence for a founder effect in invasive house finch (Carpodacus mexicanus) populations experiencing an emergent disease epidemic. Mol. Ecol. 15 (1), 263–275, http://dx.doi.org/10.1111/j.1365-294X.2005.02767.x.

Hawley, D.M., Jennelle, C.S., Sydenstricker, K.V., Dhondt, A.A., 2007. Pathogen resistance and immunocompetence covary with social status in house finches (Carpodacus mexicanus). Funct. Ecol. 21 (3), 520–527, http://dx.doi.org/10.1111/j.1365-2435.2007.01254.x.

Hawley, D.M., Dhondt, K.V., Dobson, A.P., Grodio, J.L., Hochachka, W.M., Ley, D.H., Osnas, E.E., Schat, K.A., Dhondt, A.A., 2010. Common garden experiment reveals pathogen isolate but no host genetic diversity effect on the dynamics of an emerging wildlife disease. J. Evol. Biol. 23, 1680–1688, http://dx.doi.org/10.1111/j.1420-9101.2010.02035.x.

Hickman-Davis, J., Michalek, S., Gibbs-Erwin, J., Lindsey, J., 1997. Depletion of alveolar macrophages exacerbates respiratory mycoplasmosis in mycoplasma-resistant C57BL mice but not mycoplasma-susceptible C3H mice. Infect. Immun. 65 (6), 2278–2282.

Hochachka, W.M., Dhondt, A.A., 2000. Density-dependent decline of host abundance resulting from a new infectious disease. Proc. Natl. Acad. Sci. USA 97 (10), 5303–5306, http://dx.doi.org/10.1073/pnas.080551197.

Hochachka, W.M., Dhondt, A.A., 2006. House finch (Carpodacus mexicanus) population- and group-level responses to a bacterial disease. Ornithol. Monogr. 60, 30–43.

Holt, R.D., Barfield, M., 2006. Within-host pathogen dynamics: some ecological and evolutionary consequences of transients. In: Feng, Z., Dieckmann, U., Levin, S. (Eds.), Disease Evolution: Models, Concepts, and Data Analyses, DIMACS Series in Discrete Mathematics and Theoretical Computer Science. American Mathematical Society, pp. 45–66.

Hosseini, P.R., Dhondt, A.A., Dobson, A., 2004. Seasonality and wildlife disease: how seasonal birth, aggregation and variation in immunity affect the dynamics of Mycoplasma gallisepticum in house finches. Proc. R Soc. Lond. B Biol. Sci. 271 (1557), 2569–2577, http://dx.doi.org/10.1098/rspb.2004.2938.

Hotchkiss, E.R., Davis, A.K., Cherry, J.J., Altizer, S., 2005. Mycoplasmal conjunctivitis and the behavior of wild house finches (Carpodacus mexicanus) at bird feeders. Bird Behav. 17 (1), 1–8.

Hu, Z., Yin, J., Shen, K., Kang, W., Chen, Q., 2009. Outbreaks of Hemotrophic mycoplasma infections in China [letter], Emerg Infect Dis 15(7) http://dx.doi.org/10.3201/eid1507.090174.

Hurtado, P.J., Infectious disease ecology: immune-pathogen dynamics, and how trophic interactions drive prey-predator-disease dynamics, Ph.D. Thesis, Cornell University (August 2011).

Hurtado, P., 2008. The potential impact of disease on the migratory structure of a partially migratory passerine population. Bull. Math. Biol. 70 (8), 2264–2282, http://dx.doi.org/10.1007/s11538-008-9345-y.

Kollias, G.V., Sydenstricker, K.V., Kollias, H.W., Ley, D.H., Hosseini, P.R., Connolly, V., Dhondt, A.A., 2004. Experimental infection of house finches with *Mycoplasma gallisepticum*. J. Wildl. Dis. 40 (1), 79–86.

Lange, A., Ferguson, N.M., 2009. Antigenic diversity transmission mechanisms and the evolution of pathogens. PLoS Comput. Biol. 5 (10), e1000536, http://dx.doi.org/10.1371/journal.pcbi.1000536.

Lee, K.A., 2006. Linking immune defenses and life history at the levels of the individual and the species. Integr. Comp. Biol. 46 (6), 1000–1015, http://dx.doi.org/10.1093/icb/icl049.

Lee, K., Martin, L., Wikelski, M., 2005. Responding to inflammatory challenges is less costly for a successful avian invader, the house sparrow (*Passer domesticus*), than its less-invasive congener. Oecologia 145, 243–250, http://dx.doi.org/10.1007/s00442-005-0113-5.

Ley, D.H., Sheaffer, D.S., Dhondt, A.A., 2006. Further western spread of *Mycoplasma gallisepticum* infection of house finches. J. Wildl. Dis. 42 (2), 429–431.

Lindström, K.M., Hawley, D.M., Davis, A.K., Wikelski, M., 2005. Stress responses and disease in three wintering house finch (*Carpodacus mexicanus*) populations along a latitudinal gradient. Gen. Comp. Endocrinol. 143 (3), 231–239, http://dx.doi.org/10.1016/j.ygcen.2005.04.005.

Luttrell, M., Stallknecht, D., Fischer, J., Sewell, C., Kleven, S., 1998. Natural *Mycoplasma gallisepticum* infection in a captive flock of house finches. J. Wildl. Dis. 34 (2), 289–296.

Luttrell, M.P., Fischer, J.R., Stallknecht, D.E., Kleven, S.H., 1996. Field investigation of *Mycoplasma gallisepticum* infections in house finches (*Carpodacus mexicanus*) from Maryland and Georgia. Avian Dis. 40 (2), 335–341, http://dx.doi.org/10.2307/1592229.

Marco, I., Mentaberre, G., Ballesteros, C., Bischof, D.F., Lavín, S., Vilei, E.M., 2009. First report of *Mycoplasma conjunctivae* from wild caprinae with infectious keratoconjunctivitis in the Pyrenees (NE Spain). J. Wildl. Dis. 45 (1), 238–241. (arXiv:http://www.jwildlifedis.org/content/45/1/238.full.pdf+html).

Martin II, L.B., Pless, M., Svoboda, J., Wikelski, M., 2004. Immune activity in temperate and tropical house sparrows: a common-garden experiment. Ecology 85 (8), 2323–2331, http://dx.doi.org/10.1890/03-0365.

Mikaelian, I., Ley, D., Claveau, R., Lemieux, M., Berube, J., 2001. Mycoplasmosis in evening and pine grosbeaks with conjunctivitis in Quebec. J. Wildl. Dis. 37 (4), 826–830.

Messick, J.B., 2004. Hemotrophic mycoplasmas (hemoplasmas): a review and new insights into pathogenic potential, Vet Clin Pathol 33(1), http://dx.doi.org/10.1111/j.1939-165X.2004.tb00342.x.

Osnas, E.E., Dobson, A.P., 2010. Evolution of virulence when transmission occurs before disease. Biol. Lett. 6 (4), 505–508, http://dx.doi.org/10.1098/rsbl.2009.1019.

Papazisi, L., Gorton, T.S., Kutish, G., Markham, P.F., Browning, G.F., Nguyen, D.K., Swartzell, S., Madan, A., Mahairas, G., Geary, S.J., 2003. The complete genome sequence of the avian pathogen *Mycoplasma gallisepticum* strain Rlow. Microbiology 149 (9), 2307–2316, http://dx.doi.org/10.1099/mic.0.26427-0.

Pepin, K., Volkov, I., Banavar, J., Wilke, C., Grenfell, B., 2010. Phenotypic differences in viral immune escape explained by linking within-host dynamics to host-population immunity. J. Theor. Biol. 265 (4), 501–510, http://dx.doi.org/10.1016/j.jtbi.2010.05.036.

Reynolds, A., Rubin, J., Clermont, G., Day, J., Vodovotz, Y., Ermentrout, G.B., 2006. A reduced mathematical model of the acute inflammatory response: I.Derivation of model analysis of anti-inflammation. J. Theor. Biol. 242 (1), 220–236, http://dx.doi.org/10.1016/j.jtbi.2006.02.016.

Roberts, S., Nolan, P., Hill, G., 2001. Characterization of *Mycoplasma gallisepticum* Infection in Captive House Finches (*Carpodacus mexicanus*) in 1998. Avian Dis. 45, 70–75, http://dx.doi.org/10.2307/1593013.

Segel, L.A., Perelson, A.S., 1991. Exploiting the diversity of time scales in the immune system: A B-cell antibody model. J. Stat. Phys. 63, 1113–1131, http://dx.doi.org/10.1007/BF01030002.

Simecka, J.W., 2005. Immune responses following mycoplasma infection. In: Blanchard, A., Browning, G. (Eds.), Mycoplasmas: Molecular Biology Pathogenicity and Strategies for Control, Horizon Bioscience. Horizon Bioscience, Wymondham, Norfolk, U.K, pp. 485–534. (Chapter 14).

Sydenstricker, K.V., Dhondt, A.A., Ley, D.H., Kollias, G.V., 2005. Re-exposure of captive house finches that recovered from *Mycoplasma gallisepticum* infection. J. Wildl. Dis. 41 (2), 326–333.

Sydenstricker, K.V., Dhondt, A.A., Hawley, D.M., Jennelle, C.S., Kollias, H.W., Kollias, G.V., 2006. Characterization of experimental *Mycoplasma gallisepticum* infection in captive house finch flocks. Avian Dis. 50 (1), 39–44, http://dx.doi.org/10.1637/7403-062805R.1.